UNIVERSITY OF HELSINKI REPORT SERIES IN PHYSICS

No. HU-P-D251

Effects of solar wind variations on the magnetosphere

Minna Myllys

Academic dissertation

Department of Physics
Faculty of Science
University of Helsinki
Helsinki, Finland

To be presented, with the permission of the Faculty of Science of the University of Helsinki, for public criticism in auditorium E2014 at noon (12 o'clock) on September 22th, 2017.

Helsinki 2017

Supervising professor
Professor Hannu E. J. Koskinen, University of Helsinki, Finland

Thesis supervisor
Associate professor Emilia Kilpua, University of Helsinki, Finland

Pre-examiners
Professor Kalevi Mursula, University of Oulu, Finland
Doctor Jonathan Eastwood, Imperial College London, UK

Opponent
Directrice de recherche Dominique Fontaine, École Polytechnique, France

ISSN 0359-0961
ISBN 978-951-51-2771-6 (print)
ISBN 978-951-51-2772-3 (pdf)
Helsinki University Print (Unigrafia)
http://ethesis.helsinki.fi/
Helsinki 2017

HELSINGIN YLIOPISTO — HELSINGFORS UNIVERSITET — UNIVERSITY OF HELSINKI

Tiedekunta/Osasto — Fakultet/Sektion — Faculty	Laitos — Institution — Department
Faculty of Science	Department of Physics

Tekijä — Författare — Author
Minna Myllys

Työn nimi — Arbetets titel — Title

Effects of solar wind variations on the magnetosphere

Oppiaine — Läroämne — Subject
Space physics

Työn laji — Arbetets art — Level	Aika — Datum — Month and year	Sivumäärä — Sidoantal — Number of pages
Doctoral dissertation	September 2017	127

Tiivistelmä — Referat — Abstract

The solar wind is a continuous plasma flow from the Sun into the interplanetary space. It consist of large number of charged particles that carry the solar magnetic field with it. When the solar wind reaches the Earth, it interacts with the terrestrial magnetic field and creates a magnetosphere around our planet. At times, significant plasma and energy transfer occurs from the solar wind into the magnetosphere causing strong disturbances to the Earth's inner magnetic field.

The solar wind is often considered to be a single fluid that has macroscopic measurable parameters like velocity, density, pressure and magnetic field. These parameters have a different role in controlling the solar wind-magnetosphere coupling and thus, the relative and absolute variations of the parameters affects to the magnetospheric response.

The motivation for this thesis stems from the need to improve our understanding on the solar wind-magnetosphere coupling, and thus, ultimately the space weather forecasting ability. The thesis consists of four peer-reviewed scientific publications and introduction. The main objectives were to study the coupling efficiency of different large-scale solar wind structures and how the efficiency varies with the geomagnetic latitude. This thesis also studies how the solar wind parameters control the plasma convection in the high-latitude magnetosphere. All four publications are statistical studies that combine in-situ solar wind measurements combined with the ground-based magnetometer data.

This thesis gives significant new insight on how different solar wind parameters affect the magnetospheric response. The published articles suggest that the strongest geomagnetic disturbances are caused by the solar wind structures with the combination of the high geoeffective electric field, and high solar wind velocity and dynamic pressure. Such conditions are found generally from sheath regions of coronal mass ejections. The published articles also show new observational features of well-known phenomenon, called the polar cap potential saturation, that decreases coupling between the solar wind and magnetosphere

Avainsanat — Nyckelord — Keywords
space plasma physics; solar wind; magnetosphere; geomagnetic variations

ISSN
0359-0961 Report Series in Physics

ISBN
978-951-51-2771-6 (paperback), 978-951-51-2772-3 (pdf)

HELSINGIN YLIOPISTO — HELSINGFORS UNIVERSITET — UNIVERSITY OF HELSINKI

Tiedekunta/Osasto — Fakultet/Sektion — Faculty	Laitos — Institution — Department
Matemaattis-luonnontieteellinen	Fysiikan laitos

Tekijä — Författare — Author
Minna Myllys

Työn nimi — Arbetets titel — Title

Aurinkotuulen muutoksien vaikutukset magnetosfääriin

Oppiaine — Läroämne — Subject
Avaruusfysiikka

Työn laji — Arbetets art — Level	Aika — Datum — Month and year	Sivumäärä — Sidoantal — Number of pages
Väitöskirja	Syyskuu 2017	127

Tiivistelmä — Referat — Abstract

Auringosta peräisin olevaa sähköisesti varautuneiden hiukkasten virtausta, joka kuljettaa mukanaan Auringon magneettikenttää, kutsutaan aurinkotuuleksi. Aurinkotuulen plasman vuorovaikutuksesta Maan magneettikentän kanssa muodostuu alue, jota kutsutaan magnetosfääriksi. Ajoittain vuorovaikutus johtaa myös plasman ja energian siirtymiseen aurinkotuulesta magnetosfääriin. Tämän kytkennän seurauksena Maan magneettikentässä havaitaan muutoksia, joita kutsutaan yleisesti geomagneettisiksi häiriöiksi. Geomagneettisia häiriöitä voi esiintyä paikallisesti esimerkiksi korkeilla leveyspiireillä tai häiriöitä voidaan mitata samanaikaisesti koko planeetalla.

Aurinkotuulelle voidaan määrittää erilaisia makroskooppisia parametrejä kuten esimerkiksi nopeus, tiheys, magneettikentän arvo ja paine. Näillä parametreillä on erilainen vaikutus aurinkotuuli-magnetosfäärikytkentään, joten muutokset niiden suhteellisissa ja absoluuttisissa voimakkuuksissa aiheutavat erilaisen vasteen magnetosfäärissä.

Tämä väitöskirja käsittelee aurinkotuulen eri parametrien vaikutusta magnetosfäärin. Väitöskirja koostuu neljästä vertaisarvioidusta julkaisusta ja johdannosta. Väitöskirja tutkii erityisesti, kuinka plasmaominaisuuksiltaan erilaiset aurinkotuulen suuren mittakaavan rakenteet vaikuttavat aurinkotuuli-magnetosfääri -kytkennän tehokkuuteen, millainen vaikutus eri rakenteilla on eri leveyspiirien häiriöihin sekä mitkä aurinkotuulen parametrit kontrolloivat magnetosfäärin napa-alueen dynamiikkaa.

Tässä väitöskirjassa olevat tutkimusartikkelit ovat luonteeltaan tilastollisia ja perustuvat sekä avaruusluotaimien tekemiin suoriin havaintoihin Maan lähiavaruudessa että maanpäällisten magnetometrien magneettikenttämittauksiin.

Tässä väitöskirjassa osoitettiin, että aurinkotuulen koostumuksella on merkittävä vaikutus magnetosfäärin vasteeseen. Tutkimusten perusteella aurinkotuulen rakenteet, joilla on suuren geoefektiivisen sähkökentän lisäksi korkea paine ja suuri nopeus, ajavat kaikkein tehokkaimmin suuria geomagneettisia häiriöitä verrattuna rakenteisiin, joilla on suuri sähkökenttä ja voimakas magneettikenttä.

Avainsanat — Nyckelord — Keywords
avaruusplasmafysiikka; aurinkotuuli; magnetosfääri; geomagneettiset häiriöt

ISSN
0359-0961 Report Series in Physics

ISBN

978-951-51-2771-6 (nidottu), 978-951-51-2772-3 (pdf)

Preface

I started my work towards the PhD in the University of Helsinki four years ago although in practice the journey started a long time ago when I got the idea to study physics. During the years I have received a lot of guidance and advice from more experienced researchers whose help enabled my work leading to this doctoral thesis.

First of all, I would like to emphasize my gratitude to my supervisor, Assistant Professor Emilia Kilpua, for taking me part of her research team and for the guidance and motivation. Her continuous support for my PhD project made it possible for me to complete the thesis on time. Besides my supervisor, I would like to thank Prof. Tuija Pulkkinen for sharing her immense knowledge and for her insightful remarks. My thanks also go to the other SWIFT project members.

During my PhD studies I was offered several opportunities to have a peek to other research groups abroad. Especially, I am thankful for Dr. Benoit Lavraud for his guidance and excellent teaching during my visits to The Research Institute in Astrophysics and Planetology and being easily reachable for advice even from distance. I wish to thank Dr. Lucile Turc for interesting weeks in European Space Research and Technology Centre, Netherlands. I am also grateful to Prof. James.A.Slavin for the opportunity to visit the University of Michigan and for all his advice.

I thank my previous colleagues at FMI, especially Dr. Kirsti Kauristie who provided me an opportunity to join her team as an intern and Dr. Ari Viljanen for his encouragement. My sincere thanks also goes to my co-authors Dr. Noora Partamies and Dr. Liisa Juusola.

I am thankful for the pre-examiners, Prof. Kalevi Mursula and Dr. Jonathan Eastwood, for their effort to comment and review my PhD thesis.

I would like to thank the fellow PhD students and space physics lab members in the University of Helsinki for creating an inspiring working environment.

Finally, a special and deep thanks goes to my parents and my sister for encouraging me to read and learn and for the continuous support they have given me throughout my life.

I gratefully acknowledge the Academy of Finland for the financial support of this study and Väisälä foundation, Finnish Concord Fund, the University of Helsinki Chancellor's grant, the Finnish National Doctoral Programme in Astronomy and Space physics and the University of Helsinki Doctoral Programme in Particle Physics and Universe Science to enable my international networking by travel grants.

Minna Myllys
Helsinki, 2017

Contents

List of Publications

This thesis includes an introductory part to solar wind - magnetosphere coupling and four research articles referred to as Publication 1 to 4. The introduction contains a background information for the research, data sources used in the publications and the scientific context of the results. The research articles are listed below with short summary of the author's contribution:

Publication I
Myllys, M., Partamies, N., and Juusola, L. (2015), Latitude dependence of long-term geomagnetic activity and its solar wind drivers, *Annales Geophysicae*, 33, 5, 573–581, doi:10.5194/angeo-33-573-2015
Summary: A latitude dependence of geomagnetic variations in Fennoscandia and Svalbard has been examined from years 1994 to 2010. Daily standard deviation values of the horizontal magnetic field have been used as a measure of the ground magnetic disturbance level. The focus of the study was to compare the strength of the geomagnetic variations and the timing of the geomagnetic minimum and maximum within a certain latitude band. The geomagnetic activity variations were compared with the occurrence of different large-scale solar wind drivers to show that the relative importance of different solar wind drivers differs inside the auroral (*i.e.,* high-latitude) region.
The author's contribution: Executed the data analysis, interpreted the results, produced the figures and wrote the manuscript with the help of the co-authors.

Publication II
Myllys, M., Kilpua, E., and Pulkkinen, T. (2015), Solar-wind control of plasma sheet dynamics, *Annales Geophysicae*, 33, 7, 845–855, doi:10.5194/angeo-33-845-2015
Summary: The paper studies how the varying solar wind conditions affect the energy and plasma transport in the geomagnetic tail and its large-scale configuration. The study combines solar wind measurements from the upstream of the bow shock

with the satellite data in the Earth's magnetotail. The data set consists of the years from 2008 to 2011, covering the extended low solar activity period and the rising phase of Solar Cycle 24. This allowed us to study the magnetospheric processes during relatively quiet state of the magnetosphere. Statistical maps of the sun- and tailward flows together with the occurrence of high-speed bursts during different upstream solar wind conditions are shown.
The author's contribution: Wrote the code needed to divide the data based on the solar wind values, performed the data analysis with the help of the co-authors, presented the results in international conference, produced the figures and wrote the manuscript with the help of the co-authors.

Publication III
Myllys, M., Kilpua, E. K. J., Lavraud, B., and Pulkkinen, T. I. (2016), Solar wind - Magnetosphere coupling efficiency during ejecta and sheath driven geomagnetic storms, *Journal of Geophysical Research: Space Physics*, 121(5), 4378–4396, doi:10.1002/2016JA022407
Summary: The effect of key solar wind driving parameters on solar wind-magnetosphere coupling efficiency has been investigated.The data set consists of measurements during 80 sheath and magnetic cloud driven storms. The energy input into the magnetosphere was estimated using the interplanetary electric field dawn-dusk component and two coupling functions. The energy consumption inside the magnetosphere was estimated using three different geomagnetic indices. The results highlight the differences of the coupling efficiency between different input and output parameters and discuss the possible reasons leading to the differences. The paper also studies saturation of the cross polar cap potential and how the potential is dependent on Alfvén Mach number. We found that during ICME events the saturation occurs both during low and high Alfvén Mach number conditions. The paper also introduces a method to define the time delay between the upstream solar wind measurements and the ground-based geomagnetic indices.
The author's contribution: Developed the method for the time delay analysis. Performed the data analysis. The analysis were partly executed under supervising of Dr. Benoit Lavraud during research visits to The Research Institute in Astrophysics and Planetology in Toulouse. Presented the results in international conferences, produced the figures and wrote the manuscript with the help of the co-authors.

Publication IV
Myllys, M., E. K. J. Kilpua, and B. Lavraud (2017), Interplay of solar wind parameters and physical mechanisms producing the saturation of the cross polar cap

potential, *Geophysical Research Letters*, 44, 3019–3027, doi:10.1002/2017GL072676
Summary: A statistical study of the coupling efficiency between the solar wind and the Northern Polar Cap index (PCN) has been performed. PCN is used as a proxy for the cross polar cap potential in ionosphere. The paper studies the effect of solar wind ram pressure, bulk velocity and number density to PCN index during different driving electric field and upstream Alfvén Mach number conditions. PCN is shown to be dependent on the dynamic pressure only during high solar wind driving. The paper discusses the existing saturation models and previous studies in the context of the shown results. The study highlights that it is not possible to explain all observed features of the cross-polar cap potential (CPCP) saturation with the currently existing models.
The author's contribution: Created the research plan and defined the research questions, executed the data analysis, interpreted the results and compared the results with existing models with co-authors, presented the results in international conferences, produced the figures and wrote the manuscript with the help of the co-authors.

List of Abbreviations

IMF Interplanetary magnetic field
ICME Interplanetary coronal mass ejection
GSM Geocentric solar magnetic coordinate systems
CIR Interplanetary co-rotating interaction region
HSS High-speed stream
PSBL Plasma sheet boundary layer
AE Auroral electrojet index
MHD Magnetohydrodynamics
CPCP Cross-polar cap potential
THEMIS Time History of Events and Macroscale Interactions during Substorms
KH Kelvin-Helmholtz
BBF Bursty bulk flow
DF Dipolarization front
PCN Northern Polar Cap index
DMSP Defense Meteorological Satellite Program
CF Chapman-Ferraro
IMAGE International Monitor for Auroral Geomagnetic Effects
STD Daily standard deviation
NASA National Aeronautics and Space Administration
ACE Advanced Composition Explorer
MMS Magnetospheric Multiscale mission

Introduction

Understanding and predicting space weather is becoming more and more important for the modern society. We are increasingly dependent on the satellite data and the technological infrastructures both in space and on ground that solar generated disturbances have potential to damage. The space weather in the near-Earth environment is controlled by the highly variable solar wind plasma that propagates from the solar corona into the interplanetary space. The coupling and energy transfer between the solar wind and the magnetosphere is defined by the plasma and magnetic field properties of the solar wind and the properties of the planetary magnetic field.

The details of the solar wind-magnetosphere coupling are still not fully understood. One of the open questions is how different large-scale solar wind drivers and solar wind conditions affect different magnetospheric regions. An important well-known phenomenon, which decreases the coupling efficiency between the solar wind and magnetosphere, is called the saturation of the cross polar cap potential in the ionosphere. However, the reasons leading to this saturation have, so far, remained unclear.

The motivation for this thesis stems from the urgent need to improve our understanding on the solar wind-magnetosphere coupling, and thus, ultimately space weather forecasting ability. The main scientific objective of this thesis is to study the following question: How variable solar wind drives geomagnetic storms?

This top-level research question was then divided to sub-questions that have been systematically addressed in this thesis:

1) How solar wind-magnetosphere coupling efficiency, energy and plasma transport are dependent on solar wind parameters? (**Publications II and III**)

2) What processes and parameters control the saturation of the polar cap potential (**Publications III and IV**).

3) How does large-scale solar wind driving affect the coupling efficiency and geomagnetic activity (**Publications I, III and IV)**)

This thesis is organized as follows: Chapter 1 is a brief introduction to the solar wind and the magnetosphere. Chapter 2 describes the most common energy trans-

fer mechanisms, reconnection and viscous interactions, from the solar wind to the magnetosphere. Chapter 3 discusses the effect of the key solar wind parameters to the solar wind - magnetosphere coupling. In Chapter 4, the phenomenon 'polar cap potential saturation' is introduced and the most relevant saturation models are explained. Chapter 5 reviews the geomagnetic response of the large-scale solar wind drivers and the final chapter includes the conclusions and future prospects.

1 Background

The Earth is surrounded by several different plasma environments. This Chapter introduces the basic concepts needed to understand the physical phenomena at the near-Earth space. The time varying solar wind, introduced in Sections 1 and 2, is the ultimate reason for the space weather effects observed in space and on ground. The interaction between the solar wind and the magnetosphere causes variations to the geomagnetic field. The frequency as well as the amplitude of the disturbances of the geomagnetic field are dependent on the solar wind conditions and the occurrence of its large-scale structures. Section 3 defines the term 'geomagnetic storm' as well as summaries the basic structure of the magnetosphere.

1 Solar wind

The solar wind is a plasma flow that continuously emanates from the solar corona to the interplanetary space. It consists mainly of electrons, protons and small amounts of some heavier ions. The existence of the solar wind was discovered by *Biermann* (1957) when he analysed comet tails. Later, *Parker* (1958) theoretically predicted the continuous solar wind by showing that the solar corona cannot be in a hydrostatic equilibrium. A few years later, direct spacecraft measurements confirmed the existence of the solar wind (*American Association for the Advancement of Science*, 1962). Since the beginning of space era, various spacecraft have monitored the solar wind, and its observational properties are now well understood.

The solar wind flows radially to all directions and it is both supersonic and superalfvénic near the orbit of the Earth, *i.e.,* at the distance of one astronomical unit (AU, 149 597 871 km) from the Sun. The typical velocity of the solar wind is around 350 km/s at 1 AU (e.g., *Dimmock et al.*, 2015) and it takes approximately four days for the solar wind to reach from the Sun to the Earth.

Since the solar wind is a plasma and a conductive medium, it carries the solar magnetic flux with it. The magnetic field in the solar wind is called the interplanetary magnetic field (IMF). Because the conductivity in the solar wind is nearly infinite,

Table 1: The properties of the fast and slow solar wind (*Koskinen*, 2011)

solar wind parameter	Slow wind	Fast wind
Velocity (km/s)	350	750
Electron number density (m^{-3})	1×10^7	3×10^6
Electron temperature (K)	1.3×10^3	1×10^5
Proton temperature (K)	3×10^4	2×10^5
Magnetic field (nT)	3	6
Alfvén speed (km/s)	20	70

the magnetic field is tied to the motion of the solar wind plasma, in other words, it is often said that the magnetic field is 'frozen-in' to the plasma (e.g., *Alfvén*, 1942). Since the footpoints of the IMF are connected to the surface of the rotating Sun and the field lines follow the plasma movement, the IMF forms of a spiral structure. The amplitude of the IMF is, on average, few nanoteslas at the Earth orbit (e.g., *Koskinen*, 2011).

Spacecraft measurements have revealed that the solar wind is not a homogeneous flow but it is constantly varying. The solar wind can be roughly divided into two different categories: the fast and slow solar wind (e.g., *Koskinen*, 2011). The average plasma properties of these two categories are described in Table 1. The differences between the fast and slow solar wind are due to different origin of the flows. The fast solar wind originates from the so-called coronal holes (*Bame et al.*, 1993; *Phillips et al.*, 1994). They are regions with an open magnetic field configuration, *i.e.,* the magnetic field lines extend far to the outer heliosphere where they are closed. During solar minimum, when the magnetic complexity of the Sun is decreased, the high-speed wind mainly comes from two large coronal holes near the polar regions. When the solar activity (*i.e.,* the complexity of the magnetic field) increases smaller coronal holes appear nearer to the equatorial regions and the fast solar wind flows may originate also from the lower latitudes as happend during solar cycle 23 (*Abramenko et al.*, 2010). The coronal holes are typically long-lasting structures that can last several solar rotations (e.g., *Phillips et al.*, 1994), thus the high-speed streams have 27-days periodicity in their occurrence.

The origin of the slow solar wind is more varying and currently not well understood. During solar minimum, it mainly originates near the equator from the streamer belts

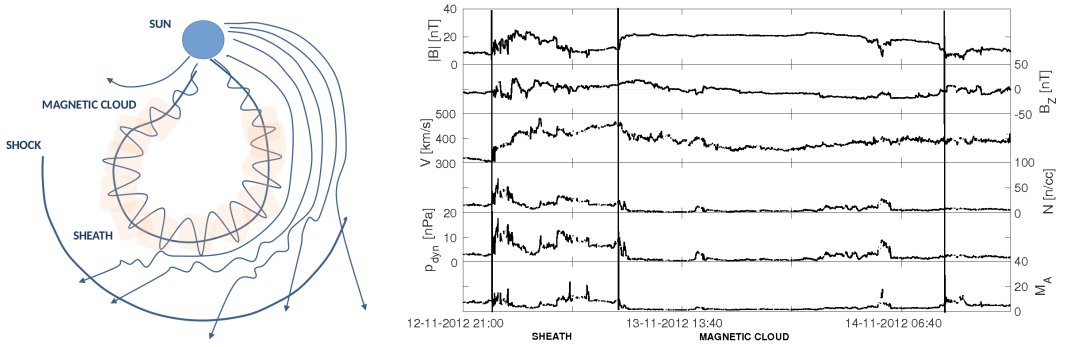

Figure 1: The structure of Interplanetary Coronal Mass Ejection (left) and spacecraft data during an ICME event (right)

2 Large-scale solar wind structures

2.1 Coronal mass ejections and their sheath regions

The strongest geomagnetic storms at the Earth are caused by the interplanetary coronal mass ejections (ICME). Coronal mass ejections are violent solar eruptions that release huge amounts of plasma and magnetic field into interplanetary space.

Because ICMEs often travel faster than the surrounding solar wind, a shock wave forms ahead of the ICME. Thus, at the Earth orbit, the ICMEs can be divided into two sub-structures with distinct solar wind properties (*Guo et al.*, 2011; *Kilpua et al.*, 2013): 1) an ejecta, which is the actual erupted magnetic structure, and 2) a turbulent sheath region between the shock and the leading edge of the ejecta (See Figure 1).

ICME ejectas can be classified based on their inner magnetic structure. The ejecta, which consists of magnetic flux rope is called a magnetic cloud (*Burlaga*, 1988). The magnetic clouds are identified by an enhanced magnetic field that slowly rotates through a large angle ($>$ 30 degrees), low proton temperatures and a low plasma beta (the ratio between the plasma pressure and magnetic pressure). The density inside the magnetic cloud is often also decreased compared to the typical solar wind conditions.

The magnetic clouds have smoother plasma parameters than the sheath regions. For example the geoeffective IMF Z-component (Geocentric solar magnetic coordinate system, GSM) may change its sign several times in a sheath region. Although, the sheath regions are shorter in durations than the magnetic clouds (**Publication**

III), they are also large-scale structures.

Figure 1 shows an example of an ICME event that consists of the sheath region and magnetic cloud. The example event occurred on 13th of November 2012 and it clearly shows the turbulent nature of the sheath compared to the ejecta part. As the sheath region consists of compressed and heated plasma it has much higher pressure, temperature and density than the magnetic cloud.

Figure 2 shows distributions of different solar wind parameters during 80 ICME events which were studied in **Publication III**. The dashed lines in the panels show the median. The distributions show that, like in the case of the example event, also statistically the sheath regions have higher density, pressure, temperature and Alfvén Mach number compared to magnetic clouds. The velocity distributions, however, are quite similar in both regions. The above-described differences in the plasma and field properties in the sheath regions and magnetic clouds affect significantly their solar wind – magnetosphere coupling efficiency and geomagnetic response. We will discuss this in Chapter 5.

2.2 High-speed streams

As discussed above, the fast solar wind ($\approx 500 - 800$ km/s at 1 AU) originates primarily from the coronal holes. The slow solar wind, on the other hand, propagates more equatorial with the velocities between 300 to 400 km/s at the Earth orbit. Because the solar wind velocity differs depending on which region it originates from, the faster solar wind flow can overtake the slower wind ahead of it forming a compression region. Such large scale-structures are rotating with the Sun and thus, called a Co-rotating Interaction Regions (CIR). Because the IMF is frozen-in to the solar wind plasma, the magnetic fields of the slow solar wind are more curved compared to the fast solar wind. The high-speed streams (HSS) and CIRs have typically a 27-day periodicity in their occurrence because the coronal holes can last for several solar rotations.

The CIR regions are identified from the spacecraft measurements using the following features: 1) solar wind flow changes from low to high, 2) proton density rises to high values near the leading edge of the stream, 3) The IMF magnitude is proportional to bulk speed with constant polarity throughout the high-speed stream part and 4) the proton temperature varies similarly to the flow speed (*Mavromichalaki and Vassilaki*, 1998).

However, there are several definitions used to recognize only the HSS events. For example the HSS has been defined to be an increase of greater than 150 km/s in the solar wind speed within a five-day interval (*Bame et al.*, 1976) or a period

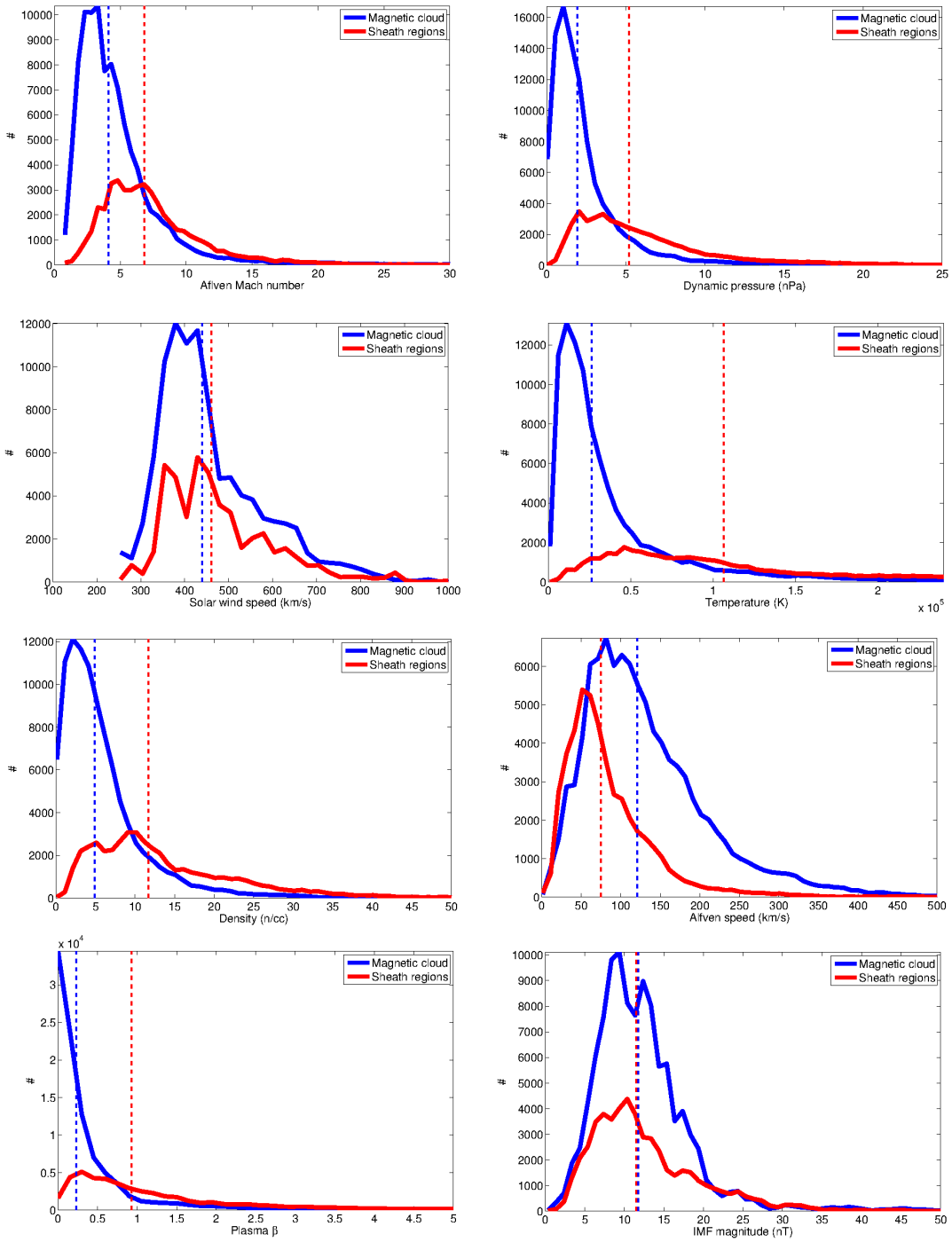

Figure 2: Distributions of 80 ICME events. The data points that are measured in the sheath regions and magnetic clouds are separated. Figure adapted from **Publication III**

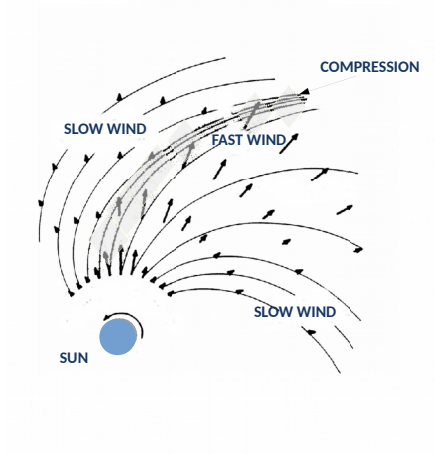

Figure 3: Formation of co-rotating interaction region and high-speed stream.

when 1-day average solar wind speed exceeds 500 km/s (*Broussard et al.*, 1978). More definitions can be found from the introduction by *Xystouris et al.* (2014). **Publication I** estimated the monthly occurrence of the HSS by counting the ratio between the times when the solar wind speed exceeded 600 km/s and the total duration of the measurements during the month.

3 Magnetosphere

The Earth has a magnetic field, which is generated by electrically conductive fluid motion in the inner part of the planet. The magnetosphere protects the Earth from the ionized particles coming from the outer space and those accelerated by the eruptions from the Sun. The region around the Earth that is dominated by its magnetic field is called the magnetosphere. Despite its name, it is not a sphere. Due to constant interaction with the solar wind, the magnetosphere is compressed on the dayside and stretches at the night to a long tail. Only the inner part of the magnetosphere (*i.e.,* the magnetic field lines nearest to the Earth) resembles a dipole field. The structure of the magnetosphere is presented in Figure 4.

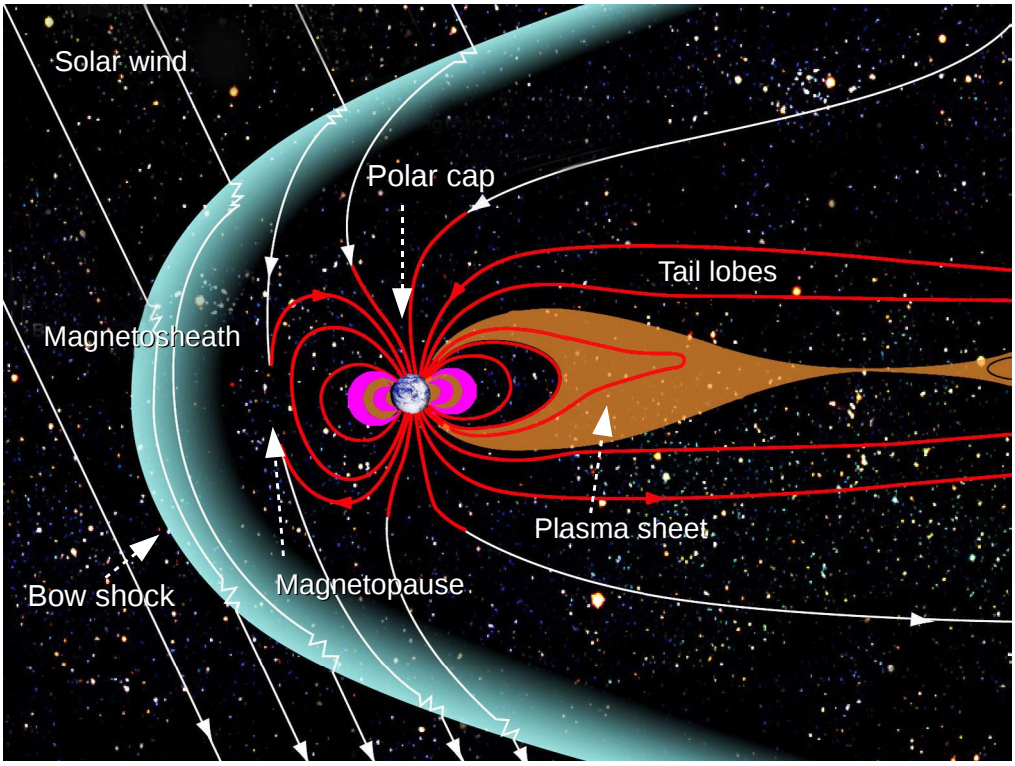

Figure 4: The structure of the magnetosphere. Courtesy: NASA

3.1 Dayside: bow shock, magnetosheath and magnetopause

The Earth's magnetic field is constantly compressed by the solar wind. In ideal case the solar wind and magnetospheric plasma do not mix and the solar wind is flowing around the magnetospheric boundary called magnetopause. In this scenario, the boundary where the solar wind ram pressure and the magnetic pressure inside the magnetosphere are equal is called the magnetopause. The standoff distance of the magnetopause on the equatorial plane can be written as (*Ridley et al.*, 2005):

$$r_{MS} = (\frac{(2B_S)^2}{2\mu_0 P_{SW}})^{1/6} \tag{1}$$

where P_{SW} is the combination of the solar wind ram pressure and the magnetic pressure. B_S is the magnetospheric magnetic field and μ_0 is vacuum permeability. From Eq. 1 it can be seen that the location of the magnetopause depends on the solar wind pressure: higher pressure leads to a more compressed magnetosphere and the magnetopause is closer to the Earth.

As explained in Section 1 in this Chapter, the solar wind at the Earth orbit is supersonic and superalfvénic. When it collides with the Earth's magnetic field, it forms a shock region in front of the magnetosphere. This shock is called the bow shock and it defines the outer boundary of the magnetospheric system. The region between the bow shock and the magnetopause is called the magnetosheath. The shock compression rate and location are dependent on the upstream solar wind Mach number. The bow shock is moved further away from the Earth when the Mach number decreases and the plasma in the magnetosheath becomes less compressed. If the magnetosonic Mach number becomes less than one, the shock disappears.

In the case of a perpendicular shock, the maximum compression ratio for the solar wind and magnetosheath magnetic fields can be written as (*Ridley et al.*, 2005)

$$\frac{B_{\text{magnetosheath}}}{B_{\text{solar wind}}} = \frac{2(\gamma+1)}{\mathrm{C} + \sqrt{\mathrm{C}^2 + 4(\gamma+1)(2-\gamma)M_A^{-2}}} \tag{2}$$

where C

$$\mathrm{C} = \gamma - 1 + 2M_S^{-2} + \gamma M_A^{-2} \tag{3}$$

M_S is the sonic Mach number (*i.e.,* solar wind speed divided by sound speed) and M_A is the Alfvén Mach number (*i.e.,* the ratio between the solar wind speed and Alfvén speed).

Thus, when the Mach numbers approach infinity and the adiabatic index (γ) is 5/3, the maximum theoretical compression ratio is 4. From Eq. 2, it follows that when the Mach number is small, the dependence between the upstream and downstream (*e.g.,* magnetosheath) magnetic fields is more non-linear than during higher Mach number periods. The shape of the magnetopause also depends on the solar wind Mach number, which affects the magnetosheath force balance as shown by *Lavraud and Borovsky* (2008). During low Mach number conditions (< 4) the magnetopause is more elangated (*i.e.,* asymmetric) in north-south direction compared to more nominal Mach number periods.

Hence, the magnetosheath consists of compressed solar wind plasma that has lower velocity and higher temperature, density and magnetic field than the upstream solar wind. The magnetosheath conditions are important in terms of solar wind-magnetosphere coupling and energy transfer because it is the magnetosheath plasma that ultimately interacts with the magnetospheric magnetic field. However, continuous spacecraft measurements are currently only available in the solar wind upstream of the bow shock.

3.2 Magnetotail: tail lobes and plasma sheet

Most of the volume of the nightside of the magnetosphere is taken by the two enormous tail lobes (See Fig. 4). The tail lobes consists of magnetically open-field lines that are connected to the surface of the Earth. The lobes are regions of magnetic field configuration parallel to the Sun-Earth line. The field lines that are attached to northern hemisphere are pointing earthward and those connected to the southern hemisphere are directed away from the Earth. The tail lobes have been measured to extend beyond 220 R_E (*Slavin et al.*, 1983).

Tail lobes are almost empty, which means that the plasma density is very low, only 0.01cm^{-3} on average (e.g, *Koskinen*, 2011). This is because, due to the open-field line configuration, the plasma is able to escape from the magnetospheric system. Due to the low density and high magnetic field value ($B = 15$ nT), the plasma beta is very small inside the tail lobes.

Between the two oppositely directed tail lobes is a denser plasma region called the plasma sheet (Fig. 4). The plasma sheet is located in the region of closed field-lines. The plasma sheet consists of two parts with slightly different plasma properties. Plasma sheet boundary layer (PSBL) separates the plasma sheet from the tail lobes. At lower latitudes is the central plasma sheet, which has a slightly higher density and weaker magnetic field than the PSBL (e.g., *Koskinen*, 2011). In the middle of the plasma sheet is a current layer, called cross-tail current. The current flows from

dawn to dusk.

The plasma sheet properties vary with the solar wind conditions. For example, periods when the density of the plasma sheet is several times higher than usual have been observed to be associated with high-density solar wind (e.g., *Borovsky et al.*, 1997). Also the thickness of the plasma sheet is varying. Under non-storm times the plasma sheet is relatively thick ($\approx 7R_E$) but it thins during substorm conditions (e.g., *Fairfield et al.*, 1981).

The plasma sheet has an important role for energy transfer inside the magnetosphere and for the auroral region because the magnetic field lines (*i.e.,* the footpoints of the dipole field) at the nightside auroral oval maps to the plasma sheet.

3.3 Magnetospheric activity

The impact of the large-scale solar wind drivers on the Earth's magnetosphere can be measured even on ground. The ground signatures of the solar wind interactions with the magnetosphere are the variations of the geomagnetic field, which can be measured using ground-based magnetometers.

Strong perturbations in the Earth's magnetic field due to the solar wind are called 'geomagnetic storms' (*Perreault and Akasofu*, 1978). The perturbations can be observed globally but sometimes they are more localized in high-latitudes and called 'substorms' (*Rostoker et al.*, 1980). The geomagnetic storm and substorm periods can be defined using the geomagnetic indices that are explained in Section 3 of Chapter 3. Typically, the geomagnetic storms are identified from the Dst index (*Sugiura and Kamei*, 1991) data, which is derived using low- and mid-latitude magnetometer stations, while the substorms can be recognized using the AE index, which is derived from high-latitude magnetometers (*Rostoker*, 1972).

The relationship between the storms and substorms is unclear but they can be considered to be different phenomena based on the different observational features. The geomagnetic storms are more rare than the substroms. The typical length of a substorm is about 2 to 3 hours (*Tanskanen*, 2009) while it may take half a day for a geomagnetic storm to develop. Substorms may occur during the geomagnetic storm but there are also so-called isolated substorms that do not occur concurrently with storms (*Baumjohann et al.*, 1996; *Tanskanen et al.*, 2002, e.g.,). During the geomagnetic storms more particles are injected into the ring current and the outer radiation belts (*Kamide*, 1998) than during the substorm. The geomagnetic storms and substorms can be both divided into three different phases, growth phase, expansion phase and recovery phase (e.g., *Rostoker et al.*, 1980; *Partamies et al.*, 2013), based on several phenomenological features.

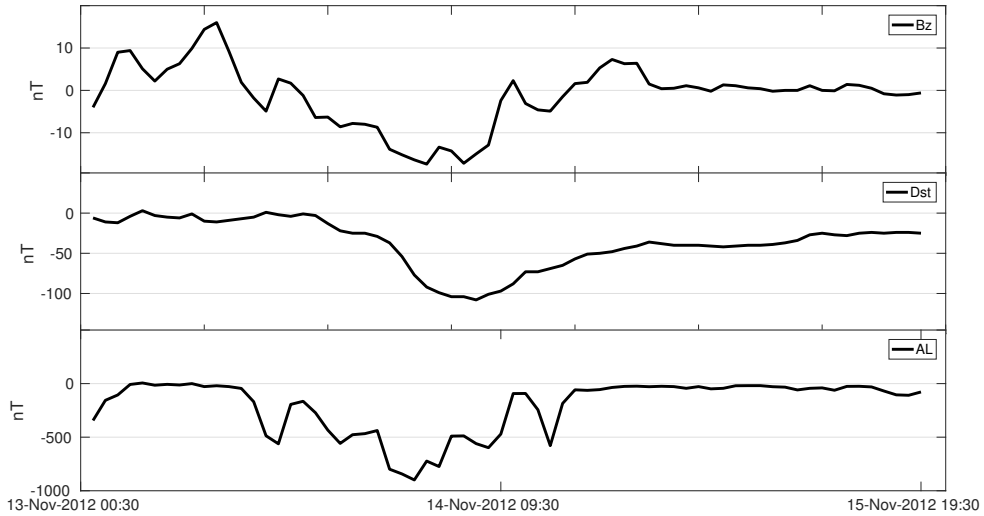

Figure 5: Geomagnetic storm caused by an ICME. The upper panel shows the solar wind B_Z component in GSM coordinates at the bow shock nose, the curve in the middle panel is the Dst index and in the lower panel the AL index.

Fig. 5 illustrates how the geomagnetic storm looks like according to Dst index: a deep drop of the index during the main phase followed by a longer recovery phase. The example storm was driven by an ICME that had a long southward B_Z period (upper panel) leading to ideal conditions for reconnection on the dayside magnetosphere. The AL index (*Rostoker*, 1972) that describes the substorm activity at high latitudes is also enhanced during the storm (bottom panel in Fig. 5).

The geomagnetic storms are often classified based on their strength, which is commonly measured using the Dst index. Even though there is no real threshold for storms, their strength is typically estimated using the Dst minimum value. For example, the storm is often called moderate when the Dst index is between -100 nT and -50 nT and intense when it goes below -100 nT (e.g., *Koskinen*, 2011).

2 Solar wind - magnetosphere coupling

As the solar wind reaches the vicinity of the Earth, it interacts with the Earth's magnetosphere and impacts the near-Earth space environment. As emphasized already in the previous Chapter, it is the magnetosheath plasma that has a direct impact to the magnetospheric magnetic field. Thus, magnetosheath plasma plays a key role of the coupling and energy transfer between the solar wind and magnetosphere. The direction and magnitude of the IMF plays a significant role when predicting the timing and amount of energy transport. This Chapter describes the phenomena and conditions that control the energy transfer between the solar wind and magnetosphere.

1 Reconnection

In magnetohydrodynamic (MHD) description of plasma, the time evolution of magnetic field (B) lines can be described using the resistive induction equation

$$\frac{\partial \vec{B}}{\partial t} = \nabla \times (\vec{V} \times \vec{B}) + \eta \nabla^2 \vec{B} \tag{4}$$

where V is the flow velocity and η is the magnetic diffusivity, which is inversely proportional to conductivity ($\eta = 1/(\mu_0 \sigma)$). In collisionless plasma diffusivity is very small, which means that the diffusivity term can be neglected from the induction equation. Thus, the magnetic field and plasma flow are frozen-in with each other and the plasma elements that are magnetically connected remain so as the plasma evolves in time.

A topological rearrangement of the magnetic field lines is called magnetic reconnection. It takes place when the 'frozen-in' condition does not hold anymore, which typically happens when some resistivity appears to the system. For example, frozen-in condition can be broken in a current sheet, which forms between two anti-parallel magnetic field configurations. The reconnection is one of the most important concepts in plasma physics because it restructures the macroscopic quantities of plasma.

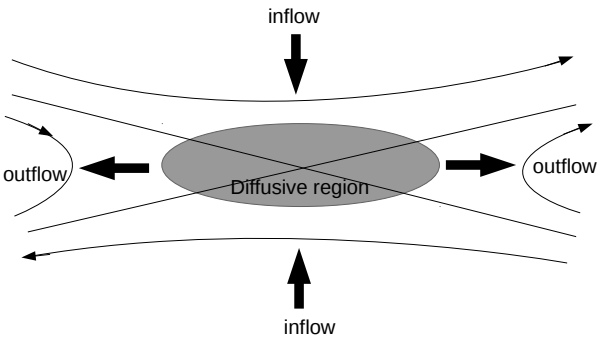

Figure 6: 2-dimensional structure of Sweet-Parker reconnection X-line. The black lines are representing the magnetic field configuration and the bolded arrows are showing the plasma inflow and outflow directions. In the middle of the diffusive region is the X-line.

Magnetic reconnection also converts magnetic energy into kinetic energy of plasma.

The early model to describe the steady-state reconnection between two oppositely directed magnetic fields on both sides of a current layer is called the Sweet-Parker model (*Parker*, 1957; *Sweet*, 1958) (See Fig. 6). The model describes the reconnection only in a qualitative manner and it does not tell anything about what actually happens in the microscopic scale in the diffusive region. However, it provides some useful scaling relations. For example, the Sweet-Parker model says that the plasma inflow speed is directly related to the Alfvén speed. Thus, the local electric field in the reconnection region is proportional to the Alfvén speed. The strength of the reconnection electric field is often called the reconnection rate.

There are two regions in the Earth's magnetosphere where the reconnection is likely to happen regularly: between the magnetosheath and magnetospheric magnetic fields on the dayside magnetopause and in the cross tail current sheet between the oppositely directed fields in the tail lobe. On average, the dayside and magnetotail reconnection are in equilibrium and the circulation of magnetic flux from the dayside to nightside and back to the dayside is called the Dungey cycle (*Dungey*, 1961).

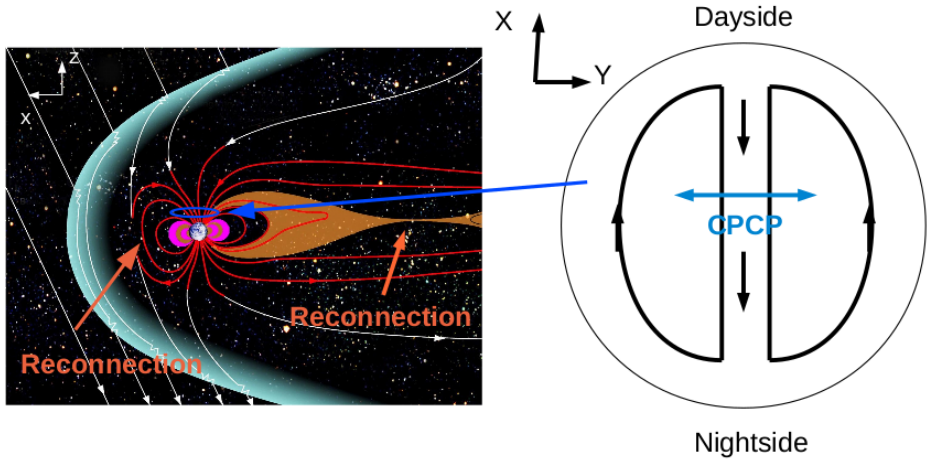

Figure 7: Dungey cycle and two cell convection pattern in high-latitude ionosphere.

In the Dungey cycle, the dayside reconnection opens the magnetic field lines at the nose of the magnetopause and the newly opened field lines are swept to the nigthside of the magnetosphere by the antisunward solar wind flow. Because of the increased magnetic flux loading the magnetotail becomes stretched and unstable. Eventually reconnection happens in the central plane of the nightside plasma sheet and the open flux becomes closed again. The closed flux proceeding to the dayside closes the Dungey cycle.

The Dungey cycle forms a two-cell convection pattern in the high-latitude ionosphere, as shown in Figure 7. At first, the plasma is convected to the nightside with the open-magnetic flux tubes across the polar cap region and then it flows back to dayside with the flux tubes that are closed due the magnetotail reconnection. The maximum potential difference between the convection pattern is the polar cap potential (CPCP).

There are some differences between the dayside and nightside reconnections. Perhaps the most notable difference is that the magnetic field strengths on the both sides of the reconnection region differ significantly from each other on the dayside. Thus, the reconnection is asymmetric. In turn, in the magnetotail, the reconnected magnetic field lines in the tail lobes have almost equal magnetic field strengths and plasma conditions.

The asymmetries in the magnetic field and plasma properties mean that the

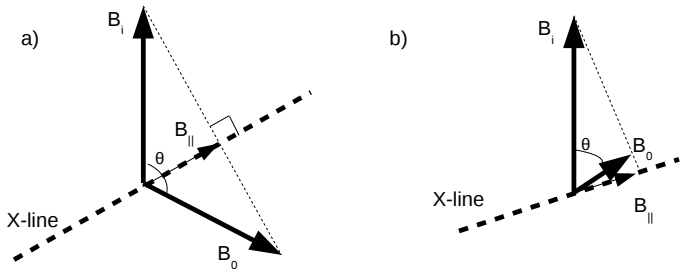

Figure 8: Orientation of the X-line when the antiparallel components of B_I and B_O exist (a) and when antiparallel components do not exist (b). The existence of antiparallel components requieres that $\cos\theta < B_O/B_I$ (See Equation 2 in *Sonnerup* (1974)). Figure is adopted from *Sonnerup* (1974)

scaling laws of the Sweet-Parker model need to be reconsidered. This has been done for example by *Cassak and Shay* (2007) who derived the reconnection rate (*i.e.,* the reconnection electric field) in terms of inner and outer magnetic fields and densities.

The other problem, which arises from the asymmetric reconnection, is that the shear angle (the angle between the magnetosheath magnetic field and the magnetospheric magnetic field directions) must be large (*i.e.,* between $90° - 180°$) for the reconnection to take place. This was shown by *Sonnerup* (1974) who considered an X-line orientation where both the inner and outer reconnected field lines have a common component ($B_{\|}$) along the X-line. Thus, the magnetic field components perpendicular to the X line (*i.e.,* $B_{\perp,O}$ and $B_{\perp,I}$) on the two sides of the reconnection region participate to the reconnection (Fig. 8). As shown by *Sonnerup* (1974), the existence of such anti-parallel components depends on the ratio of the magnetic field strengths (B_O/B_I). According to Equation 2 in *Sonnerup* (1974) the reconnection can only take place when the shear angle is high, if the ratio B_O/B_I is small, which is the case on the dayside magnetopause.

The above-described scheme is called the 'component reconnection' (*Sonnerup*, 1970, 1974). It assumes that reconnection takes place first at the subsolar magnetopause before stretching along the magnetopause and the X-line is tilted with respect to the equatorial plane. The tilt angle is defined by the shear angle that roughly equals to the IMF clock angle (the relation between the IMF B_Y and B_Z components) on the nose of the magnetopause.

There is also another theory of the location of the reconnection on the dayside magnetopause. It is called anti-parallel hypothesis, and it states that the reconnection only happens in the regions were the magnetic fields inside and outside of the magnetopause are antiparallel (*Luhmann et al.*, 1984). The both hypotheses, component reconnection and anti-parallel reconnection, have got support from the spacecraft measurements and the dominant mechanism seems to depend on the IMF orientation (*Trattner et al.*, 2007).

The reconnection point in the neart-Earth magnetotail, which is part of the Dungey cycle, is statistically located around $20 - 30$ R_E from the Earth (*Nagai et al.*, 1998). This location was also confirmed by **Publication II** by studying the directions and magnitudes of the plasma sheet flows using data from Time History of Events and Macroscale Interactions during Substorms (THEMIS) mission spacecraft (*Angelopoulus*, 2009).

2 Viscous interactions

Before Dungey proposed his model, *Axford and Hines* (1961) suggested that the observed plasma convection pattern in the ionosphere is caused by viscous interaction between the outer boundary of magnetosphere and the solar wind flow when the magntopause is fully closed. The collisional viscosity at the magnetopause is weak while the finite gyroradius with the wave-particle interaction causes some level of anomalous viscosity. Viscous interactions are estimated to provide roughly 10% of the momentum transfer from the solar wind to the magnetosphere (e.g., *Koskinen*, 2011).

Most of the energy and mass transport into the magnetosphere occurs during the southward IMF because of reconnection. However, there are also other mechanisms than reconnection for the energy and mass inflow, like Kelvin-Helmholtz (KH) waves. The KH waves belong to the viscous interactions and can lead to a considerable mass transfer into the magnotail (*Nykyri and Otto*, 2001). The KH instability is a fluid phenomenon related to the velocity (V) shear between two fluid surfaces, for example the solar wind flow along the Earth's magnetopause may give rise to KH vortices.

In the ideal MHD description, the onset condition for the KH instability is (e.g., *Foullon et al.*, 2008)

$$[\vec{k} \cdot (\vec{V_1} - \vec{V_2})]^2 > \frac{n_1 + n_2}{\mu_0 m_p n_1 n_2} [(\vec{k} \cdot \vec{B_1})^2 + (\vec{k} \cdot \vec{B_2})^2] \tag{5}$$

where 1 and 2 refer to fluids on the opposite sides of the boundary (for example in the magnetosheath and in the magnetospheric plasmas), n is the number density and

m_p is the proton mass. V_1 and V_2 are velocities tangential to the layer. The equation above tells immediately that the instability is caused by the velocity shear, $|\vec{V_1} - \vec{V_2}|$. The instability condition is most likely to be fulfilled when the wave propagation is parallel to the high flow shear and when B_1 and B_2 are nearly parallel or anti-parallel. Such conditions are typically met along the magnetospheric flanks. The KH unstable region is depended on the IMF clock angle (*Foullon et al.*, 2008).

3 Solar wind control of the coupling efficiency, energy and plasma transport

The coupling and energy transfer between solar wind and magnetosphere are not constant but vary in time due to varying solar wind conditions. As discussed earlier the transition of the solar wind plasma and magnetic field through the bow shock into the magnetosheath is an important factor when determining the solar wind - magnetosphere coupling efficiency and the plasma and energy transport.

In this Chapter the solar wind control of the energy and plasma transfer in the plasma sheet is discussed. The Chapter also gives a brief introduction how the times of energy inlow into magnetosphere as well as the magnetospheric response are estimated using measurements.

1 Energy and plasma transfer in the plasma sheet

The ideal MHD description of large-scale plasma convection from the dayside across the polar cap to the nightside and then back to the dayside (i.e. the Dungey cycle) gives an impression of smooth plasma flow in the nightside plasma sheet. Most of the time the plasma sheet convection is indeed dominated by slow speed (< 100 km/s) flows that circulate the plasma around the Earth towards the dayside (*Juusola et al.*, 2011). The slow flow pattern is not significantly depended on the IMF orientation (*Wang et al.*, 2006). However, the greatest part of the mass and energy is carried during short duration bursty bulk flow (BBF) events (*Angelopoulus et al.*, 1992, 1994).

High speed flows occur in bursts which can last less than 10 seconds (*Baumjohann et al.*, 1990). The BBFs are defined as intervals of plasma flow speed > 100 km/s in the plasma sheet when the flow exceeds 400 km/s for at least 5-sec interval (*Angelopoulus et al.*, 1992, 1993). The BBFs are typically part of flow enhancement intervals that last of the order of 10 minutes. Fast flow in the plasma sheet is thought to indicate the near-Earth reconnection. *Juusola et al.* (2011) showed that statisti-

cally IMF clock angle controls the high-speed flows while the solar wind electric field plays only a minor role.

The high-speed bursts typically occur near the midnight meridian (*Baumjohann et al.*, 1990) and the flows with speed > 500 km/s are almost always directed strictly towards the Earth (*Juusola et al.*, 2011). BBFs are often accompanied by dipolarization fronts (DFs) (*Nakamura et al.*, 2002) that are common features of substorm dynamics. DFs are defined to be sharp increase of B_Z (the north-south magnetic field component) which is preceded by a transient decrease in B_Z. The DFs are considered to be a signature of an abrupt change from a stretched to a more dipolarized magnetotail configuration. DFs are also described to be Earthward moving flux tubes with lower entropy compared to the ambient plasma sheet (*Pontius and Wolf*, 1990). *Fu et al.* (2012) observed that the maximum occurrence rate of DFs and substorms are comparable, which indicates relationship between the two.

Figure 9 is adapted from the **Publication II** and it shows THEMIS (*Angelopoulus*, 2009) observations of the occurrence of the fast speed flows in the magnetotail plasma sheet during years 2008-2011. The color panel shows the percentage of observations during which 1-min averaged flow speed exceeds 50 km/s (upper panels) or 100 km/s (lower panels). The data set is divided into two groups based on the sign of the V_X component (GSM) to show the sunward and tailward flows separately. Figure 9 demonstrates that the flows exceeding 100 km/s are relatively rare and predominantly pointing to sunward direction. The flows also brake significantly when the radial distance from the Earth decreases. The high-speed flows have been suggested to slow down when they reach from the tail-like field to more dipolar field plasma sheet (*Shiokawa et al.*, 1997).

The other large-scale magnetic field configurations frequently observed in the magnetotail are flux ropes. The flux ropes consist of helical magnetic field configuration. They can be identified from the bipolar B_Z signature and a peak in the B_Y component, which represents the core field of the rope. Like DFs, flux ropes have also been observed embedded within Earthward or tailward high-speed flows (*Slavin et al.*, 2003). Flux ropes are signs of multiple reconnection X-lines and they are observed frequently in the tail between -15 to -30 R_E (*Slavin et al.*, 2003).

In **Publication II** it was found that the occurrence of the fast tailward flows ($|V_{\text{tail}}| > 100$ km/s) does not significantly vary with the solar wind conditions like the sunward fast flows do. The IMF B_Z had the most significant impact to the plasma sheet flows, which is understandable in terms of the Dungey cycle. It was also observed that, surprisingly, the fast flow bursts were more common during the slow solar wind (< 400 km/s) than fast solar wind. The reason for this is unclear

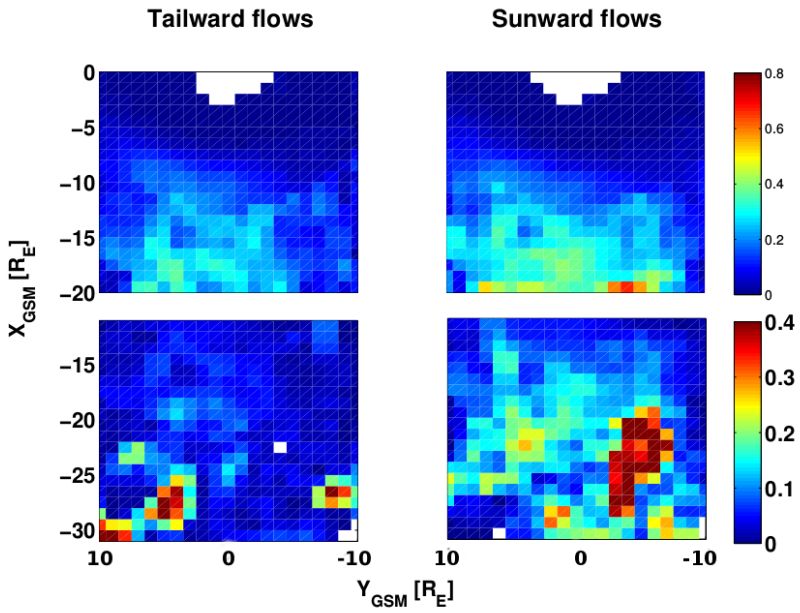

Figure 9: THEMIS observations of the magnetotail plasma sheet flows during years 2008-2011. Percetage of observations during which 1-min averaged flow speed exceeds 50 km/s (100 km/s) are shown in the upper (lower) panels. The studied region in the upper and lower panels are partly overlapping. The data set is divided into two groups based on the sign of the V_X component. Figure adapted from **Publication II**

and it should be examined more in detail in the future.

2 Coupling parameters and functions

The solar wind-magnetosphere coupling can be studied using both observations and simulations. The simulations provide better tools to study the coupling on large-scales while the point measurements are important in space weather predicting point-of-view and to verify the simulation results. The problem that arises when using the point measurements is that it is impossible to get a global view of the system. This means that, the amount of energy transferred from the solar wind into the magnetosphere cannot be directly measured and proxies are needed to estimate the level of coupling and the times of the energy inflow.

During the last two decades the spacecraft have offered continuous measurements of the solar wind. Several coupling functions have been developed to describe the geoefficiency of the solar wind. A comprehensive list of different coupling functions and parameters suggested in the literature can be found from Table 1 by *Newell et al.* (2007). The coupling functions use the upstream solar wind parameters and most of them aim at describing the electric field value that impinges to the magnetopause (*Kan and Lee*, 1979; *Akasofu*, 1981). They are combinations of the solar wind velocity and magnetic field.

The *Kan and Lee* (1979) function is an estimate for the reconnection electric field on the dayside magnetopause nose. It is derived using the component hypothesis of the reconnection (*Sonnerup*, 1974) (see Chapter 2 Section 1) and purely geometrical approach. The function is $E_R = VB_T\sin^2(\theta/2)$, where V is the solar wind velocity, B_T is tangential interplanetary magnetic field and θ is the shear angle that is typically estimated using the IMF clock angle. The function has been used in **Publication IV** to estimate the reconnection electric field.

One of the best coupling functions in the literature, when measured by the correlation with several geomagnetic indices, has been developed by *Newell et al.* (2007). The coupling function can be written as

$$\frac{d\Phi_{\mathrm{MP}}}{dt} = V^{4/3}B_T^{2/3}\sin^{8/3}(\frac{\theta}{2}) \tag{6}$$

where Φ_{MP} is the magnetic flux on the dayside magnetopause, V and B_T are the same as in the case of reconnection electric field (E_R) and θ is the IMF clock angle. The function represents the rate of magnetic flux, which is open at the magnetopause.

The derivation of the Newell function is based on the previous coupling functions in the literature. The exponents of the solar wind parameters have been extracted

by a correlation study with 10 different geomagnetic indices characterizing magnetospheric activity. The study was made using a large data set covering measurements over two solar cycles. The Newell function, like the most coupling function in the literature, ignore the role of the magnetosheath in the coupling process.

Borovsky (2008) used a completely different approach while deriving his coupling function. He started from the assumption that reconnection is a local process and is determined by the local plasma parameters. He used a formula, derived by *Cassak and Shay* (2007), as a basis for the function. The Cassak-Shay formula defines the local reconnection rate using four free parameters that are the magnetospheric and magnetosheath magnetic fields and number densities. *Borovsky* (2008) presented all of these parameters, except the magnetospheric number density (ρ_m), using the upstream solar wind parameters. He used the shock jump conditions and MHD simulations for the parameterization. *Borovsky* (2008) also included one extra free parameter, the IMF clock angle (θ), to his function. As a result, the coupling function is derived completely independently from the magnetospheric measurements and it takes into account the magnetosheath dynamics. The Borovsky function is

$$\mathrm{R} = 0.4\mu_0^{1/2}\sin(\frac{\theta}{2})\rho V^2(1+0.5M_{MS}^{-2})(1+\beta_S)^{-1/2} \cdot [C\rho+(1+\beta_S)^{-1/2}\rho_m]^{-1/2}[(1+\beta_S)^{1/2}+1]^{-1/2} \quad (7)$$

where ρ is the solar wind number density, M_{MS} and M_A are the magnetosonic and Alfvén Mach numbers, V is velocity, β_S is the magnetosheath plasma beta ($\beta_S = 3.2\cdot 10^{-2}M_A^{1.92}$) and C is the compression ratio of the bow shock $C = [[1/4]^6 + [1/(1+1.38log_e(M_A))]^6]^{-1/6}$.

The functional form of the Borovsky function differs significantly from the other coupling functions (see Table 1 by *Newell et al.* (2007) for comparison). The Borovsky function also depends on the upstream Mach numbers, which makes it unique.

Borovsky (2008) presented a correlation study between his new coupling function and commonly used geomagnetic indices. The correlation study was also done using the other coupling functions, like the Newell function, to demonstrate that the Borovsky function shows nearly as good results as the Newell function despite the different derivation approach.

Guo et al. (2011) executed a statically study of the geomagnetic storms caused by the ICMEs and their sheath regions and showed using superposed epoch analysis that Borovsky and Newell functions give similar profiles for the energy input estimates but their results significantly differ at times when dynamic pressure is high or Alfvén Mach number is low. Because the ICME ejecta typically has a very low Alfvén Mach

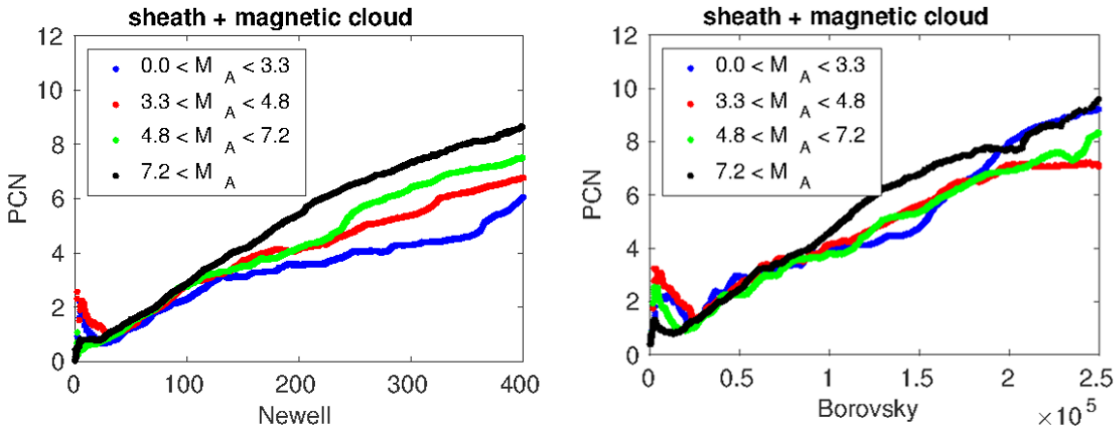

Figure 10: The geomagnetic PCN index as a function of Newell and Borovsky function during four different Aflvén Mach number levels. The data points cover 80 ICME events. See the details of the Figure from **Publication III**

number, the coupling function to describe the geoefficiency of the ejecta should be selected with a caution.

The **Publication III** studies the solar wind-magnetosphere coupling efficiency during the 80 ICME driven geomagnetic storms. The effect of the different solar wind driving parameters was examined separately. The energy input rate was estimated using the Newell and Borovsky functions. According to the results, the Borovsky function gives more linear energy estimate into the magnetosphere for all solar wind conditions compared to the Newell function. Consistently with the results by *Guo et al.* (2011), the Newell and Borovsky function differed the most during low Alfvén Mach number solar wind. Figure 10 is adopted from **Publication III** and it shows the PCN index (See next Section) as a function of Newell and Borovsky functions during four different Aflvén Mach number levels. When the Newell function experiences clear saturation during the lowest Aflvén Mach number intervals, the Borovsky function shows less non-linearity.

3 Geomagnetic indices

3.1 High-latitude indices: AE and PCN

Northern Polar Cap index (PCN) is measuring the perturbation of the horizontal magnetic field in the polar cap region in the northern hemisphere. The index is derived from a single ground-based magnetometer station located in Thule in Greenland. The index is based on the papers by Troshichev (*Troshichev et al.*, 1979, 1988).

Troshichev et al. (1996) showed that the PCN index correlates well with the CPCP measured by the Defense Meteorological Satellite Program (DMSP) satellites. Thus, the PCN has been used as a proxy for the CPCP in the **Publication III and IV**. The index is available over several solar cycles with a 1-minute time resolution, which makes it ideal for statistical studies. There are also empirical formulas that are showing the relationship between the CPCP in kV and PCN (*Ridley et al.*, 2004). However, it should be noted that the correlation studies between the CPCP and PCN have been done during relatively low solar wind electric field conditions and thus, new studies are needed to ensure the correlation also during high solar wind electric field driving.

The PCN index saturates when the solar wind driving is strong enough (**Publications III and IV)**, and the reason for the saturation is most likely related to the CPCP saturation explained in Chapter 4.

Another index describing the geomagnetic field perturbations in the high-latitudes is called the auroral electrojet (AE) index. It was originally derived by *Davis and Sugiura* (1966) and it is designed to be a measure for the electrojet activity at the auroral ionosphere (See Fig. 11). AE is widely used index to describe the evolution of geomagnetic substorms and to measure the general level of magnetic variations at high latitudes. It is derived using the horizontal perturbations of geomagnetic field from 12 magnetometer stations (*Rostoker*, 1972). The AE index is defined as AE = AU-AL, where AL represents the maximum magnetic perturbation generated by the westward electrojet and AU is the maximum perturbation caused by the eastward electrojet. These indices, AL and AU, can also be used separately since they may vary independently from one another (*Rostoker*, 1972).

The AE index can be considered to have a two-component structure. The first component is related to perturbations in the directly driven two-cell convection pattern in ionosphere, like PCN, and the other component is related to the formation of substrom current-wedge (*Kamide and Kokubun*, 1996). This means that the index starts to increase relatively quickly after solar wind conditions change favorable to dayside reconnection. The other intensification of the index happens when the tail-

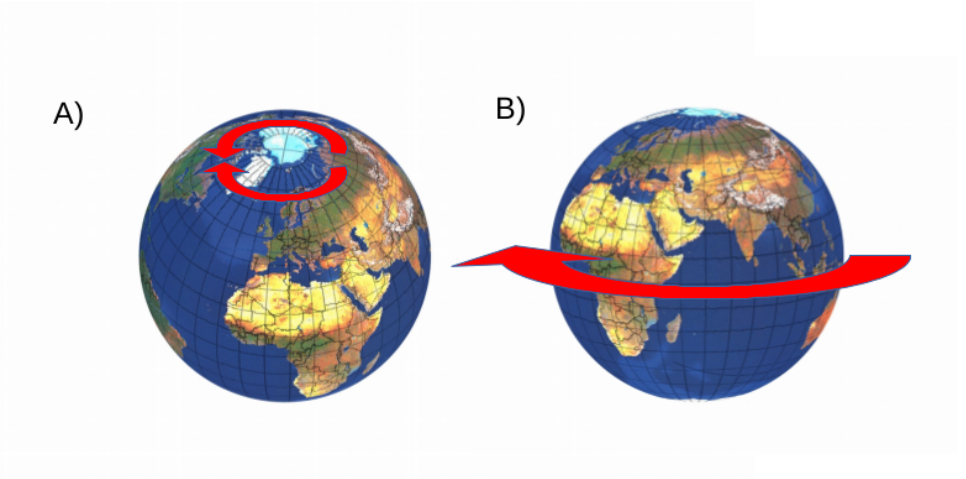

Figure 11: Illustration of location of the auroral electojets flowing from noon to midnigth at the auroral ionosphere (A) and the ring current (B) that lies in the equatorial plane and circulates clockwise.

side reconnection begins. This behavior is clearly present in the time delay analysis, which was done in **Publication III**.

The problem related to the AE index is that it saturates during high solar wind driving (showed in **Publication III**). The reason for saturation can be related to the saturation of the auroral electrojets due to the CPCP saturation (*Weimer et al.*, 1990), but it is also affected by the expanding auroral oval. In **Publication III**, it was found that the AE index starts to show non-linearity around the same E_Y values as PCN. This suggests that during the moderate electric field driving, the saturation of the AE index is related to the CPCP saturation.

3.2 Ring current indices: Dst and SYM-H

Geomagnetic storms are often defined using a geomagnetic index, called Dst (*Sugiura and Kamei*, 1991), which describes the perturbation in the horizontal geomagnetic field components. The Dst index is derived from the ground-based magnetic field measurements observed at low latitudes. It is based on the measurements from four different magnetometer stations called Hermanus (33.3° south, 80.3° in magnetic dipole latitude and longitude), Kakioka (26.0° north, 206.0°), Honolulu (21.0° north, 266.4°), and San Juan (29.9° north, 3.2°). The Dst index is considered to react to

the ring current activity (Fig. 11), and especially to reflect the symmetric part of the current.

The Dst index is computed at 1-hour intervals, which limits its usefulness in studies that require higher time resolution. Thus another index, like SYM-H (*Iyemori*, 1990), is needed to resolve higher-frequency variations. The SYM-H has 1-minute time resolution and can be used as a high-resolution Dst index (*Wanliss and Showalter*, 2006). SYM-H is derived using six magnetometer stations (See the list in Table 1 by *Wanliss and Showalter* (2006)). Like Dst, SYM-H also reacts to the symmetric part of the ring current.

Publication III uses the SYM-H index to describe the ring current evolution during ICME driven storms. The ring current has a long memory and it builds up slowly after strong solar wind interaction. Thus, the SYM-H has a long time delay before it responses to the changes in driving solar wind conditions as shown in **Publication III**. The SYM-H does not saturate when the solar wind driving increases (**Publication III**), which may be a sign that ring current does not saturate either (see also discussion in *Lopez et al.*, 2009).

4 Solar wind - magnetosphere coupling efficiency

The energy transfer between the solar wind and the magnetosphere leads to intensification of magnetospheric and ionospheric current systems, which can be observed by variations in the geomagnetic field data. Certain solar wind parameters correlate well with the geomagnetic disturbances, like B_Z and E_Y. The role of these parameters to the geomagnetic activity is relatively easy to understand, because both of them have a role in the magnetic reconnection at the magnetopause nose. Like explained in Chapter 2 reconnection at the dayside magnetopause typically occur when the magnetic fields are nearly anti-parallel, which is the case when the IMF points southward. The E_Y, on the other hand, is a proxy for the reconnection electric field. Thus, the amount of energy available (*i.e.,* the energy input) and times when the energy is transferred from the solar wind into the magnetosphere are often estimated using E_Y, B_Z or coupling functions (e.g., *Turner et al.*, 2009; *Guo et al.*, 2011).

The magnetospheric response (*i.e.,* the energy output) is typically estimated using the geomagnetic indices as discussed in the previous Section. The geomagnetic indices can be used to estimate the energy dissipation via ring current, auroral precipitation and Joule heating using empirical relationships (See *e.g., Turner et al.* (2009)) or just to estimate geomagnetic variations in some certain latitude band (*Partamies et al.*, 2009). The solar wind - magnetosphere coupling efficiency are

typically defined as:

$$\text{coupling efficiency} = \frac{\text{energy output}}{\text{energy input}} \tag{8}$$

The coupling efficiency for the same driver and similar solar wind conditions may differ when different definition is used (**Publication III**). As demonstrated in previous studies, some solar wind structures are more geoeffective at high latitudes while others have higher impact to the global disturbance level and to lower latitudes (*Huttunen et al.*, 2004, 2006).

In **Publication III** the coupling efficiency was defined using three different proxies for the energy input (E_Y, Newell and Borovsky functions) and three different geomagnetic indices for the energy output (PCN, AE and SYM-H). The results showed that the Borovsky function gives the best estimates for the energy input when the above-mentioned indices were used, which is most probably related to the fact that the function includes the Mach number. The results also highlighted the difference of geomagnetic variations in the polar region (PCN) and lower latitudes (SYM-H) by showing that the PCN saturates in certain solar wind conditions while SYM-H does not.

5 The magnetospheric response time

One thing that one needs to consider when studying the coupling between the solar wind and magnetosphere is the time delay between the solar wind observations and the geomagnetic response. This must be taken into account when selecting the most suitable definition for the coupling efficiency. The magnetosphere has also been noted to act like a low-pass filter, (*Clauer et al.*, 1981; *Takalo et al.*, 2000; *Ilie et al.*, 2010) which means that it does not react to all small-scale solar wind fluctuations. Thus, solar wind parameters can be either averaged (**Publication III and IV**) or integrated (*Turner et al.*, 2009; *Yermolaev et al.*, 2012) in time.

Publication III focused on this time delay issue. A new method to solve the time delay and the averaging window length was developed. The method tries to maximize the correlation between solar wind measurements and geomagnetic indices. The method defines the time delay to be the time difference between the cause (input) and response (output). The averaging time window is used to smooth the input data and it is centered to the time step in question. The method uses the following procedure to determine the delay and the averaging window length:

1. The correlation coefficient (r) is calculated between the used input and output parameters when the time window is kept fixed and the time lag is varied

2. Computed correlation coefficients are stored into matrix elements so that each column represents different time lag and each row different the time window value

3. The time window length is changed and the correlation coefficients are computed again by varying the time lag

4. New correlation coefficients are again stored into the matrix

Before starting the procedure, the maximum value for the time delay must be selected. Since the time window is centered to the time step in question, the maximum possible value for the window length is twice the time delay. The above-mentioned steps are repeated until the maximum time window length is achieved. The most optimal time delay and averaging window length are defined to be the coordinates for the matrix element whose correlation coefficient value is the highest.

There are few things that need to be taken into account when the method is used. The definition for the correlation coefficient can be selected freely but it is important to pay attention to the differences between the definitions (*Artusi et al.*, 2002). In **Publication III**, the time delay method was executed using Spearman's rank correlation coefficient since it is a nonparametric measure and it describes the monotonic increase between the variables. The other option would be, for example, Pearson correlation coefficient but since it is a parametric method and assesses the linear instead of monotonic trend between the variables, it is not as suitable to a situation where some non-linearity may occur between the variables.

The time intervals, which are used in the time delay analysis, should also be carefully chosen. The ideal solar wind structures for the method are those that last more than an hour to get enough data points for the study and that have some large-scale fluctuations in the input parameters. In **Publication III**, it was noted that the magnetic cloud intervals are not suitable for the method. The reason is their relatively smooth inner structure and thus, the correlation coefficient does not vary much when the time delay and the window length are varied. The sheath regions, on the other hand, are ideal for the method.

Figure 12 shows an example of the result of the time delay analyses used in **Publication III**. The example analysis was done between the Borovsky coupling function and the PCN index. The color of each bin shows Spearman's correlation coefficient. The horizontal axis is the time lag and the vertical axis is the time

window length. In the example case, the highest coefficient is achieved when the time delay is 17 minutes and the window length is 27 minutes. The defined time delay is compatible with the previous studies in literature that have found, for example, 20 minutes time delay between the reconnection electric field (*i.e.,* Kan-Lee function (*Kan and Lee*, 1979)) and the PCN (*Stauning and Troshichev*, 2008) index and 15 minutes time lag between the CPCP and IMF Z-component (*Eriksson et al.*, 2000).

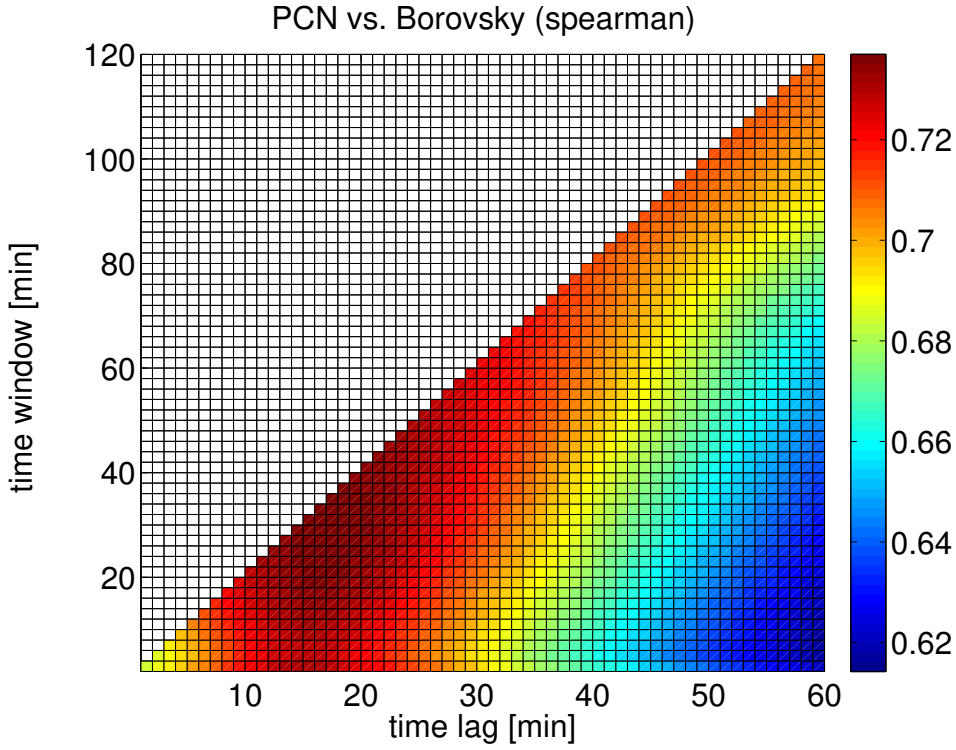

Figure 12: Example of the time lag and the averaging time window length determination. The correlation coefficients between the Borovsky function and PCN index are computed using measurements in 80 sheath regions. The horizontal axis shows the used time lag values and the vertical axis the averaging time window lengths. The time resolution is 1 minute.

4 Saturation of the polar cap potential

One well-known phenomenon that weakens the coupling between the solar wind and the magnetosphere is called 'polar cap potential saturation'. This Chapter defines what is meant by the polar cap potential saturation and it gives a brief summary of the saturation models suggested in the literature.

1 Polar cap potential saturation

The reconnection potential along the merging line at the dayside magnetopause can be mapped into the high-latitude ionosphere along the equipotential magnetic field lines. Thus, in theory, the CPCP should match with the assumed reconnection potential. Typically, it is also assumed that the reconnection electric field could be estimated using the upstream solar wind parameters, namely the dawn-dusk component of the interplanetary electric field (E_Y).

If we expect that both of the above-mentioned assumptions are correct, we should be able to observe a linear dependence between the E_Y and the CPCP. This means that the CPCP should always increase with increasing E_Y. However, this is obviously not the case. Non-linearity between the CPCP and the E_Y has been noted in several studies (*Reiff et al.*, 1981; *Reiff and Luhmann*, 1986; *Weimer et al.*, 1990; *Russell et al.*, 2001; *Ridley et al.*, 2005; *Shepherd*, 2007; *Wilder et al.*, 2011). The non-linear relationship of the CPCP and the E_Y is illustrated in Figure 13.

The linear dependence between the E_Y and the CPCP would mean that the reconnection electric field at the magnetopause scales as the solar wind upstream electric field and that the reconnection electric field is fully reflected into the ionosphere. Thus, the saturation of the CPCP implies that one or both of the above assumptions are violated. The reasons why these assumptions do not always hold can, for example, be related to the magnetosheath properties (*Lavraud and Borovsky*, 2008; *Lopez et al.*, 2010; *Wilder et al.*, 2015). The conditions in the magnetosheath are largely dictated by the solar wind transition past the bow shock, which in turn, is governed by the solar wind parameters. For example, the compression ratio at the

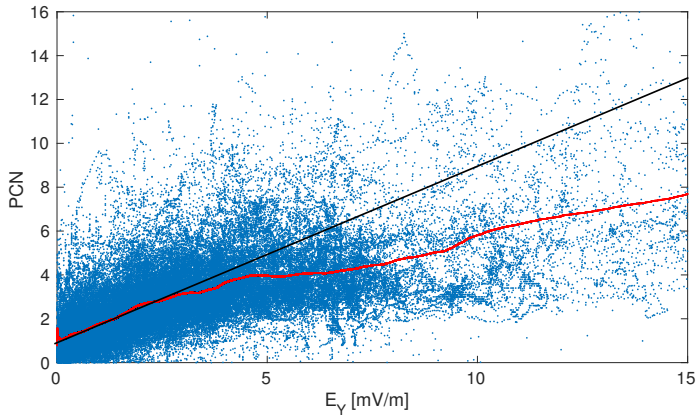

Figure 13: PCN index, a proxy for the CPCP, as a function of the E_Y. The blue dots show 1-min measurements during 80 ICME interactions and the red curve is the smoothed average of PCN. The black line represents the best-fit line between PCN and the E_Y.

shock depends on the Magnetosonic Mach number. The strength of the shock (and the compression of the magnetosphere) increases with the increasing Mach number.

The change in the plasma and field conditions from the solar wind to the magnetosheath are not the only factors violating the linear assumptions. The saturation can also be related to the changes in the reconnection rate (*Hill et al.*, 1976; *Raeder and Lu*, 2005) or some inner magnetospheric mechanisms (*Hill et al.*, 1976; *Siscoe et al.*, 2002b). The following sections discuss the solar wind parameters, which have been observed to affect the CPCP value and the possible mechanisms leading to the saturation.

2 Solar wind parameters affecting the polar cap potential

Saturation is typically defined as a non-linearity between the solar wind E_Y and the CPCP because their relationship can be easily understood theoretically. However, as can be seen from Figure 13 there is a lot of scatter in the data points throughout the whole E_Y range. The saturation as well as the high scatter of the data both raise the question of the role of the other plasma parameters in controlling the CPCP value.

Several studies have noted that the solar wind Alfvén Mach (M_A) number seems to have a significant role in the CPCP saturation and that the saturation occurs

predominantly during the low (< 4) M_A conditions (*Ridley et al.*, 2005; *Kivelson and Ridley*, 2008; *Lavraud and Borovsky*, 2008; *Lopez et al.*, 2010; *Wilder et al.*, 2011, 2015). *Lavraud and Borovsky* (2008) studied the magnetosheath during a low M_A solar wind using MHD simulations, and concluded that during those periods the magnetosheath flows along the flanks of the magnetopause are enhanced. The increased magnetic forces squeeze the magnetopause on the flanks. Since the size and shape of the whole magnetosphere and the thickness of the magnetosheath change as a response to the solar wind M_A, it is likely that M_A can affect the CPCP as well.

Ridley et al. (2005) pointed out that the bow shock compression ratio is M_A depended, thus it should be taken into account when estimating the CPCP. Both *Lavraud and Borovsky* (2008) and *Lopez et al.* (2010) noted that the magnetosheath plasma beta and thus, the magnetosheath force balance, are significantly different during low M_A conditions compared to nominal or high M_A periods. They both suggested that the reason for the saturation is in the altered magnetosheath flows due to low plasma beta (See section 3.2). Another low Alfvén Mach number related mechanism that could decrease the coupling efficiency between the solar wind and the magnetosphere is the impedance mismatch of the solar wind across the polar cap and the ionosphere (*Kivelson and Ridley*, 2008).

Consistently with the previous studies, it was shown in **Publications III and IV** that CPCP saturates during the low M_A conditions using the PCN index as a proxy for the CPCP. Both studies, however, showed evidence that the saturation is not only related to low M_A but the saturation is also visible during higher M_A periods. This introduces an important new question regarding whether the low M_A saturation is only one of the several saturation mechanisms or whether there is a saturation mechanism, yet not completely understood, that can explain the saturation over a wider range of M_A conditions.

Previous studies in the literature do not have a consensus on the role of the solar wind dynamic pressure to the CPCP. Dynamic pressure plays a role for example on determining the reconnection X-line length at the dayside magnetopause since it controls the compression of the magnetosphere. Because the reconnection potential at the magnetopause is the electric field integrated along the X-line, the shrinkage of the X-line length should decrease the potential (*Raeder and Lu*, 2005). Dynamic pressure also defines the pressure balance between the solar wind and magnetosphere and thus, defines the location of the magnetopause standoff distance. The so-called 'Hill-Siscoe' saturation model, discussed in the next Section, is based on the pressure balance and the magnetopause currents and it predicts that during high E_Y conditions, the solar wind dynamic pressure increases the CPCP value that contradicts the X-line prediction.

Wilder et al. (2011) showed using a large data set that non-linearity of the CPCP from the linear fit has statistically significant correlation with the M_A but not with the solar wind dynamic pressure. The study implies that dynamic pressure is hardly the main reason for the CPCP saturation. However, **Publication IV** showed that the dynamic pressure has an increasing effect to PCN during high solar wind electric field values but no dependence during low and moderate solar wind driving. Thus, it is likely that the solar wind dynamic pressure is one source of the scatter of the data points especially in the saturation regime.

The saturation of the CPCP is often considered to be a phenomenon occurring only during southward IMF periods, since the CPCP is largely caused by the plasma convection in the high-latitude ionosphere driven by the dayside subsolar reconnection. However, reconnection also happens during the northward IMF. During the northward IMF the reconnection occurs at higher latitudes near the cusps (e.g., *Luhmann et al.*, 1984). The relative importance of the viscous processes to the energy transport is also increased during the northward IMF. The changes in the energy transport during the northward IMF modify the large-scale plasma convection pattern in the ionosphere. Instead of two convection cells, like in the case of southward IMF, there are four cells (*Wilder et al.*, 2008). Two of the cells are driven by the viscous interactions and the other two, called reverse convection cells, by the lobe reconnection (*Crooker*, 1992). *Wilder et al.* (2008) showed that the potential across the reverse convection cells also saturates (*i.e.,* exhibits non-linearity) and later, several other studies have reported similar results (*Sundberg et al.*, 2009; *Bhattarai et al.*, 2012).

3 Polar cap potential saturation models

In the literature several different mechanisms have been suggested to explain the linear and non-linear behavior of the CPCP during different solar wind driving conditions. However, the cause of the saturation is still unclear and even the details related to the saturation are under debate. The CPCP saturation has remained a controversial topic for such a long time because it has turned out to be difficult to test the different models. These difficulties arise from the limited amount of measurements covering the saturation regime, because the saturation mainly occurs during high solar wind driving ($E_Y > 3$ mV/m). In this Section some of the best known saturation models are introduced.

3.1 The Hill-Siscoe formulation

The Hill-Siscoe model is based on three different publications (*Hill et al.*, 1976; *Siscoe et al.*, 2002a,b). The main idea of the model is that the CPCP saturation is caused by a so-called feedback mechanism where the increased reconnection rate on the dayside magnetopause causes changes to the current systems in the inner magnetosphere.

Siscoe et al. (2002a) created a saturation model based on the work done by *Hill et al.* (1976). The model states that the CPCP saturates at times when the Region 1 currents are significantly enhanced due to the increased solar wind driving. The main idea of the model is that during the times when reconnection occurs at the dayside magnetopause, the Region 1 current system is fed by the MHD generator (*Lundin and Evans*, 1985), which transforms kinetic energy to electricity. The resulting strong Region 1 currents create a magnetic field that opposes the Earth's dipole field at the dayside magnetopause. This leads to a weaker magnetospheric magnetic field, and finally lowers the reconnection rate by limiting the Aflvén speed at the reconnection site.

The assumption that the dayside magnetic field would be significantly decreased due to Region 1 currents has been questioned. *Lavraud and Borovsky* (2008) showed using global MHD simulations that the enhanced Region 1 currents do not lower the magnetic field near the reconnection site. The weakening of the dayside magnetosphere causes only the magnetopause to move closer to the Earth. To maintain the pressure balance with the solar wind, the Chapman-Ferraro (CF) currents at the magnetopause must get stronger and thus, the CF currents increases the magnetospheric magnetic field just inside the magnetopause. Thus, the magnetic field at the magnetopause is set by the pressure balance with the solar wind.

The contradiction between the pressure balance and the first version of the Hill-Siscoe model was also noted by *Siscoe et al.* (2002b). Thus, the model was improved and the authors suggested that the reason for the CPCP saturation lies in the current limited Region 1 system instead of lowered reconnection rate. This mechanism has been called as a 'ram pressure model' in the literature (*Borovsky et al.*, 2009). As mentioned previously, the dayside MHD generator feeds the Region 1 currents when the solar wind driving increases. According to the model by *Siscoe et al.* (2002b), the current required to provide the $J \times B$ -force needed at the magnetopause to sustain the balance with the solar wind, sets the upper limit for the Region 1 currents. *Siscoe et al.* (2002b) noticed that at the saturation limit, the CF currents at the magnetopause were absent and the Region 1 currents had replaced their role in acting against the solar wind pressure. Thus, the Region 1 system is not able to close any more current without violating the pressure balance condition.

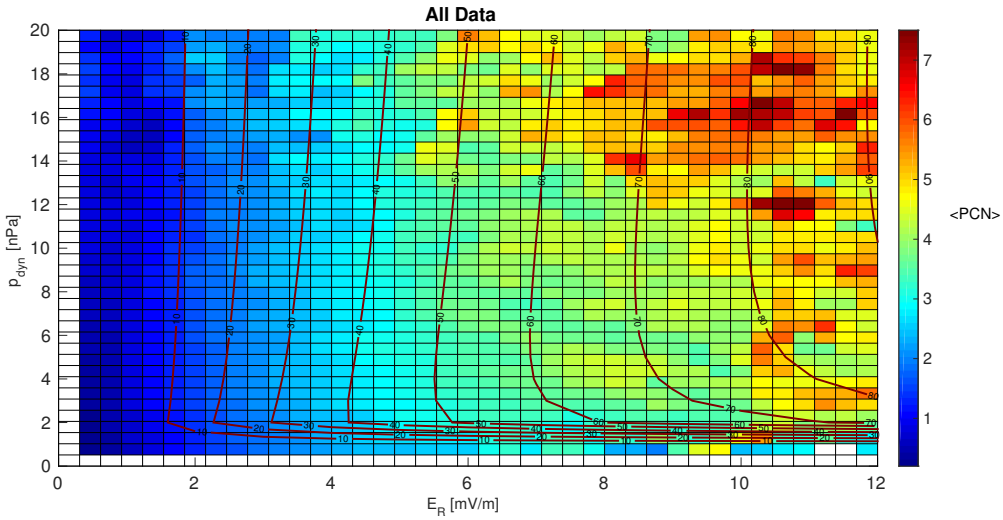

Figure 14: PCN index as a function of dynamic pressure and reconnection electric field (E_R). The curves top of the color map shows the Hill-Siscoe prediction for the cross-polar cap potential in kV. The Hill-Siscoe prediction is based on the equation 6 in *Siscoe et al.* (2002b). We have also adopted the values for the coefficient ξ (3.6) that parametrizes the geometry of current flow lines in the ionosphere and for the ionospheric conductance (12 Siemens) used in *Siscoe et al.* (2002b). Figure is published as Online Supplementary Material with **Publication IV**

Because the maximum strength of the Region 1 currents depends on the pressure balance, the saturated CPCP must depend on the solar wind dynamic pressure. The formula for the CPCP derived by *Siscoe et al.* (2002b) depends on the pressure (p_{dyn}) in the following way:

$$\Phi_H = 57.6 p_{dyn}^{1/3} \cdot E_R / (p_{dyn}^{1/2} + 0.01 \xi \Sigma \cdot E_R) \tag{9}$$

where Σ is the ionospheric conductance, ξ is the parameterizing coefficient and E_R is the reconnection electric field. The functional form of the Hill-Siscoe model was compared with the observations in **Publication IV**, where PCN was used as a proxy for the CPCP. Even though the measured PCN increases with the dynamic pressure during high solar wind driving, the formula fits poorly to the data when E_R and p_{dyn} are high as can be seen from Figure 14.

3.2 The magnetosheath force balance model

It is ultimately the magnetosheath plasma and electric field that interacts with the magnetic field of the Earth. Thus, the magnetosheath dynamics plays a key role when energy is transferred into the magnetosphere.

When the solar wind plasma and IMF propagate in the magnetosheath their stream paths are diverted. This can also have significant effect on the field and plasma properties that impinges on magnetopause. The changes in the magnetosheath flow pattern must be taken into account when predicting the CPCP according to *Lavraud and Borovsky* (2008) and *Lopez et al.* (2010). Only the plasma streamlines with flows across the merging line at the magnetopause affect the CPCP.

In MHD, the force balance in the magnetosheath is described by the momentum equation. When the time-independent flow is considered, the equation is:

$$\rho(\vec{V} \cdot \nabla)\vec{V} = \vec{J} \times \vec{B} - \nabla\vec{p} \tag{10}$$

where ρ is mass density, V is velocity, B magnetic field, J current density and p pressure of the plasma fluid. The pressure gradient and $J \times B$ are the forces defining the path of the flow streamlines within the magnetosheath (*Lopez et al.*, 2010). Both of these forces act to divert the streamlines around the magnetosphere but the significance of the diversion depends on the relative strength of the forces. Most of the time the magnetosheath flows are dominated by the pressure gradient (*Lavraud and Borovsky*, 2008; *Lopez et al.*, 2010). However, there are times when the impact of the $J \times B$-force becomes equal or even dominant compared to the pressure gradient. The variations in the force balance affect the large-scale magnetosheath flow pattern.

The parameter that describes the force balance in the magnetosheath is the plasma beta. The plasma beta in the magnetosheath is strongly controlled by the bow shock properties that in turn depend on the sonic and Alfvén Mach numbers in the upstream solar wind. The evolution of the plasma parameters across the shock can be described by the Rankine-Hugoniot jump conditions. As shown by *Lavraud and Borovsky* (2008) in their Fig. 2a, the magnetosheath beta decreases below one when the Mach number is below 4. To create the figure, *Lavraud and Borovsky* (2008) varied the magnetic field from 1 to 30 nT and used a constant value for the upstream velocity (650 km/s), density (1cm^{-3}), adiabatic index (5/3) and ion and electron temperatures (50000K). *Lavraud and Borovsky* (2008) used relatively slow density and temperature values, because those are typical for magnetic clouds (See Fig. 2), which cause the most severe geomagnetic storms.

When the magnetosheath plasma beta decreases below one, it means that the

magnetic forces are enhanced and the significance of the $J \times B$ term in the momentum equation increases. Thus, the flows are diverted around the magnetopause more than during the times when the pressure gradient dominates (*Lavraud and Borovsky*, 2008; *Lopez et al.*, 2010).

The magnetosheath flow pattern during high and low plasma beta conditions are illustrated in Figure 15. The flow diversion decreases the total amount of flux that enters the reconnection region. Thus, even if the flow elements are carrying more flux, due to the increased magnetic field, the potential drop across the magnetopause does not increase with the upstream electric field. In other words, due to the decrease of the geoeffective length of the plasma crossing the magnetopause during low magnetosheath plasma beta conditions, the CPCP has a non-linear response to the upstream electric field.

In addition to the flow diversion, the magnetosheat plasma beta is also suggested to be related to the ability of the magnetic flux tube to derform as a response to the magnetosheath flows as it is carried over the polar cap (*Wilder et al.*, 2015). The deformation follows from the fact that when the open flux tube formed by the dayside merging is carried over the polar cap, they are affected by the collisional drag force in the ionosphere caused by the ion-neutral particle collisions. The drag force resists the motion of the foot point of the flux tube. The other end of the flux tube is connected to the solar wind and the magnetosheath and it flows towards the magnetotail. Because of the collissional drag force that is antiparallel to the magnetosheath flows, the magnetic flux tube is bent (*Strangeway et al.*, 2000). The field line bending provides a tension force that can act against the collisional drag and accelerates the foot points in the ionosphere.

Figure 16 demonstrates the effects of the open field line bending. The Figure 16A illustrates a 2-D (Z-Y plane in GSM system) plot of the open-closed field line boundary. Inside the polar cap region, the magnetic field is perturbed to sunward direction (*i.e.,* out of the page) due the tailward magnetosheath flows while outside the polar cap the field is perturbed to antisunward direction due to return flow of the closed field lines. The magnetic shear at the open-closed field line boundary leads to formation of a current system that is associated with the Region 1 field-aligned currents.

Figure 16B shows how the currents are coupled with the ionosphere and magnetopause. The current system that is created by the bending of the open field lines, is closed via ionospheric horizontal current and the magnetopause current (green lines). The horizontal ionospheric current causes the force ($J \times B$) that acts against the collision drag force, while the $J \times B$ at the magnetopause is slowing down the bulk magnetosheath flow. According to *Strangeway et al.* (2000) the steady-state

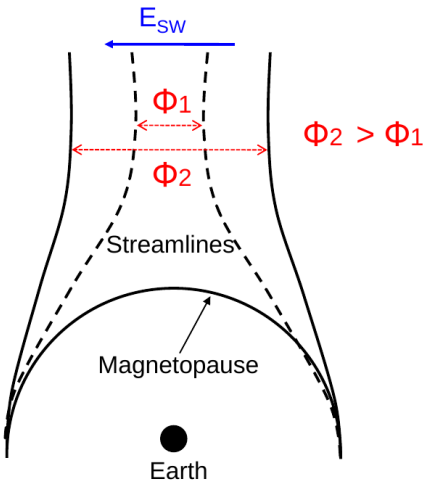

Figure 15: Illustration of the magnetosheath flow pattern during high (black lines) and low (dashed lines) magnetosheath beta. The magnetic flux (Φ) that encounters the magnetopause when magnetosheath beta is high is greater than the flux during low beta conditions. Courtesy: Dr.Benoit Lavraud

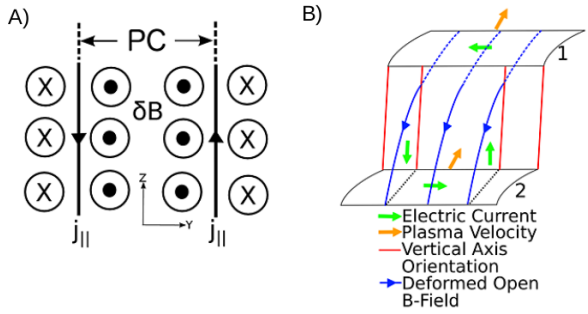

Figure 16: Panel A: Magnetic shear at the open-closed field line boudary and the associated field-aligned currents (j). PC means polar cap. The Figure is showing ZY-plane in the in GSM coordinates and is viewed from the Sun. The magnetic perturbation force is pointing antisunward in inside PC and sunward outside the PC. The Figure is adopted from *Wilder et al.* (2015). Panel B: Deformation of the magnetic flux tubes. The Figure is also viewed from the Sun. The 1 refers to magnetopause and 2 to the ionosphere. Diagram is adapted from *Strangeway et al.* (2000)

plasma velocity in the ionosphere, is directly related to the magnetic perturbation in the bent flux tube that, in turn, has linear dependence with the magnetosheath convection electric field. This steady-state scheme for the coupling is expected in the linear regime of the CPCP.

Based on the formula for the ionospheric plasma velocity by *Strangeway et al.* (2000), it is clear that if the magnetic flux tube bending saturates, so does the ionospheric convection and thus, the CPCP. The hypothesis proposed by *Wilder et al.* (2015) is that the ability of the flux tubes to bend depends on the magnetosheath plasma beta which governs the stiffness of the flux tube. The stiffer the flux tube is, the less it can bend. According to the MHD simulations by *Wilder et al.* (2015) the flow diversion predicted by *Lavraud and Borovsky* (2008) and *Lopez et al.* (2010) and flux tube deformation occur in tandem.

Since the saturation during low Mach number conditions is found both in statistical studies based on measurements (*Ridley et al.*, 2005; *Lavraud and Borovsky*, 2008; *Wilder et al.*, 2011) and MHD simulations (*Lavraud and Borovsky*, 2008; *Lopez et al.*, 2010; *Wilder et al.*, 2015), there is strong support for the magnetosheath force balance models. The advantage of both of the saturation mechanisms that depend

on the magnetosheath beta (*i.e.,* flow diversion and magnetic field bending) is that they can explain the saturation both during the southward and during northward IMF. The problem with the models comes from the fact that they are not able to predict the possible saturation during more nominal Alfvén Mach number conditions (**Publication III and IV**).

3.3 The other suggested mechanisms

The magnetosheath force balance model is not the only model that attempts to explain the CPCP saturation using low upstream Alfvén Mach number conditions. *Ridley* (2007) and *Kivelson and Ridley* (2008) have explained the saturation using the so-called Alfvén wings.

Alfvén wings are formed during sub-Alfvénic solar wind when the magnetic field starts to bend when it encounters an obstacle (*Neubauer*, 1980). The bending launches Alfvén waves which propagate with the Alfvén speed (v_A) along the magnetic field lines. The plasma flow still affects the magnetic field lines and the Alfvén waves travel with an angle $\theta = \text{atan}(M_A^{-1})$. The interaction with the flow velocity and the Alfvén wave creates a cavity in which flow characteristics are different than in the surroundings. The electric field within the wing is lower than within the medium, which may be the reason for the saturation.

The formation of the Alfvén wings at the Earth's magnetosphere using MHD simulations was studied by *Ridley* (2007) who showed that the CPCP saturation occurs near the point when the solar wind becomes sub-Alfvénic. The analysis was later extended by *Kivelson and Ridley* (2008) to define the CPCP using the solar wind and ionospheric properties. The idea behind the CPCP expression is that the impedance difference between the solar wind and ionosphere causes the signal propagating into the ionosphere to partially reflect. This reflection can be observed as a saturation. The problem with the Alfvén wing model is that the Alfvén Mach numbers are assumed to be very small, even below one. Such values are very rarely encountered in the near-Earth solar wind. However, the statistical study by *Wilder et al.* (2011) and **Publications III and IV** revealed the saturation even in conditions when the Alfvén Mach number was considerably larger than the Alfvén wing theory requires.

Observational evidence of the Alfvén wings at the Earth has been offered by *Chané et al.* (2012). However, *Chané et al.* (2012) observed Alfvén wings when the solar wind was sub-Alfvénic due to low density and not due to high IMF like expected by *Ridley* (2007).

5 Large-scale solar wind structures and geomagnetic activity

Large-scale solar wind structures, like ICMEs and HSSs, collide with the Earth's magnetosphere and cause geomagnetic perturbations. The previous chapters have focused on how single solar wind parameters affect to the magnetospheric system and explained that the solar wind-magnetosphere coupling is different depending on the solar wind conditions. Since the inner structure of the drivers differs, as explained in Chapter 1, there are also statistically discernible differences between the impact of the drivers.

The definition of solar wind- magnetosphere coupling efficiency also differs, as mentioned in Chapter 3 in Section 4. This is because there are several current systems in the magnetosphere, which have a different response to solar wind driving. The occurrence rate of the drivers depends on the phase of the solar activity cycle, and thus, the relative importance of different drivers also varies in time. The following sections focus on the observed differences in the magnetospheric response of the large-scale drivers and the latitude dependence of the relative importance of the drivers.

1 Geoeffectiveness of large-scale solar wind structures

Most of the previous papers in the literature have been studying the differences between the ICME-driven and CIR-driven storms (e.g., *Gonzalez et al.*, 2002; *Richardson et al.*, 2002; *Borovsky and Denton*, 2006; *Turner et al.*, 2009). The CIRs are closely related to HSSs. The solar wind conditions during the ICME and CIR driven storms are typically different. For example, during the CIR interactions with the magnetosphere the IMF B_Z does not remain steady, as is often the case with ICMEs (*Turner et al.*, 2009). *Borovsky and Denton* (2006) compiled a comprehensive list (Table 1 in their publication) of the important differences between the ICME and CIR driven storms. The list includes, for example, the following remarks: during

the ICME interactions 1) magnetosonic Mach numbers are smaller, 2) bow shock compression ratios are lower and 3) magnetosheath beta is lower compared to CIR interactions.

Turner et al. (2009) also studied the geoeffectiveness of the ICME and CIR driven storms and showed statistically meaningful differences in the energy coupling and partitioning between the two drivers. The study included 280 storms in total covering an entire solar cycle from 1995 to 2004. The energy input was estimated using the epsilon parameter (*Akasofu*, 1981) integrated over the storm period and the energy output was the sum of the integrated value of energy dissipated via ring current, auroral precipitation and Joule heating. According to *Turner et al.* (2009) ICME-driven storms have on average much greater electromagnetic energy input (measured by the epsilon parameter), deeper Dst reduction and higher dissipated energy in the case of all energy sinks. However, when the ratio of the energy output and input was computed, the CIR events had a higher coupling efficiency than the ICME events. The difference of the efficiencies was statistically significant. Thus, even though there is more energy available during the ICME than CIR driven events, the energy transfer is not more efficient.

Most of the intense geomagnetic storms (Dst < -100 nT) are associated with ICMEs (e.g., *Richardson et al.*, 2001; *Huttunen et al.*, 2002). *Turner et al.* (2009) did not separate the effect of the two ICME sub-structures (*i.e.,* the sheath and ejecta) while studying the geomagnetic response. The importance of the sheath region alone for generating the magnetic storms was pointed out by *Huttunen et al.* (2002). Later, *Yermolaev et al.* (2012) also demonstrated the importance of sheath regions for driving geomagnetic storms.

Huttunen et al. (2002) noted that ejecta-related storms drove a strong Dst depletion more often than sheath- or shock-related storms and in the case of strong Kp variations the situation was vice versa. *Huttunen et al.* (2004) showed that low- and high-latitude activity do not always occur concurrently and sheath and magnetic clouds can have different response of the auroral and ring current systems.

There is also asymmetry in the low-latitude evolution of the geomagnetic field during the sheath- and magnetic cloud driven storms that can be seen when the SYM-H and ASY-M indices are studied. *Huttunen et al.* (2006) showed that ASY-M index (*i.e.,* asymmetric part of ring current) dominated during sheath driven storms compared to magnetic cloud driven storms. Thus, like *Huttunen et al.* (2004) concluded, several magnetic indices are needed to have a global idea of the magnetospheric effects because the response of the ring current and the ionosphere can vary by the type of the solar wind driver.

When the statistical differences between the sheath regions and magnetic clouds

(See Figure 2 in Chapter 1) and the results of the **Publication III** are considered, it is evident that they have different responses in the magnetosphere. The ring current builds-up and the Dst index response slowly after the solar wind driving has increased. The sheath regions may have at times as strong magnetic fields as the magnetic clouds, but due to the fluctuating nature and the short duration of the region, they do not have as high impact to the ring current as the magnetic clouds.

Previous studies, like *Huttunen et al.* (2002), noted that the sheath regions have a higher impact to the high-latitude geomagnetic indices. This is easy to understand in terms of the **Publications III and IV**. The magnetic clouds have statistically more often M_A below 4 and the CPCP saturation favours low M_A conditions. The dynamic pressure is also typically much larger in the sheath regions than magnetic clouds. According to the **Publication III** the higher dynamic pressure leads to higher response in the polar region. Both higher M_A and dynamic pressure values are factors that favour greater high-latitude response during the sheath regions than during the magnetic clouds.

2 Long-term variations of geomagnetic activity

Geomagnetic storms can be observed throughout the solar cycle, even though the number of storms is higher during the solar activity maximum (*Zhang et al.*, 2006). As shown by several authors, the occurrence of the ICMEs and HSSs is dependent on the solar cycle phase (*Gonzalez et al.*, 2002; *Richardson et al.*, 2002; *Georgieva et al.*, 2006; *Holappa et al.*, 2014): the number of ICMEs peaks near the solar maximum while the HSS maximum is during the declining phase of solar cycle. Because of the solar cycle dependence of the solar wind drivers, also the geomagnetic variations vary during the cycle phase. The importance of the HSS of driving geomagnetic storms increases during the declining phase (*Gonzalez et al.*, 2002; *Georgieva et al.*, 2006). Figure 17 is adopted from **Publication I**. It visualizes the occurrence of the ICME (third panel) and high solar wind speed (second panel) with the solar cycle (i.e. sunspot number, top panel) during the years studied in **Publication I**.

Georgieva et al. (2006) studied the years from 1992 to 2002 and compared the average and cumulative geoeffectiveness of HSS and magnetic cloud driven storms. They noted that the geoeffectiveness of magnetic clouds have a strong solar cycle dependence unlike the HSS. The authors suggested that the decreased efficiency is related to the fact that for magnetic clouds, both the magnitude of the magnetic field and the velocity, have a solar cycle dependence. For the HSS, the authors did not observe variations of geoefficiency with the solar cycle phase. However, the

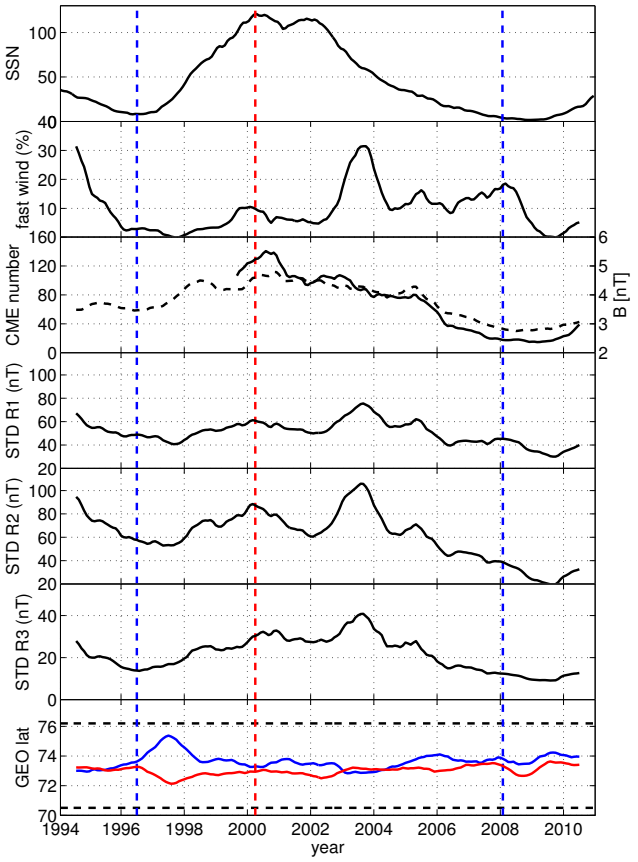

Figure 17: From top to bottom: number of sunspots, the percentage of the time when solar wind speed exceeds 600 km/s, the number of ICMEs (solid) together with the IMF magnitude (dashed), STDs in the northermost latitude band (R1, 73.06° – 75.25° MLAT), STDs in middle band (R2, 63.55° – 67.34° MLAT) and STDs in the southermost band (R3, 56.89° – 60.99° MLAT), and the maximum geographic latitudes of the maximum eastward (blue) and westward (red) electrojet current densities in degrees. The studied time interval is from 1994 to 2010. In every panel the values are 13-month smoothed averages. The black dashed horizontal lines in the bottom panel show the southern boundary of R1 (upper line) and the northern boundary of R2 (bottom line). The blue dashed vertical lines shows the starting and ending point of solar cycle 23 and the red dashed line show the month of the smoothed maximum sunspot number. See details from **Publication I**.

cumulative efficiency of the both drivers to the geomagnetic variations depends on the abundance of the drivers. For example, during the time interval studied by *Georgieva et al.* (2006) the yearly sum of the daily Dst index got its minimum in the same year as the maximum number of magnetic clouds but the yearly sum of the Kp index (*Mayaud*, 1980) peaked one year earlier than the HSS occurrence.

Because different solar wind drivers have a different impact to different current system and thus, to different latitude bands (*Finch et al.*, 2008) the solar cycle effect to the occurrence of the drivers also means that the geomagnetic perturbations may peak in different latitudes at different times (*Echer et al.*, 2004).

Holappa et al. (2014) studied using principal component analysis the latitudinal distribution of annual geomagnetic activity in 1966-2009. According to the analysis, the first two principal components describe more than 97% of the variance in annually averaged geomagnetic activity. While the first principal component represents the global geomagnetic activity caused by mixture of solar wind drivers (like ICME and HSS), the second component describes how the latitudinal distribution of geomagnetic activity deviates from the global activity and it correlates with the relative annual fraction of HSS. *Holappa et al.* (2014) showed that the second mode peaks at auroral latitudes (corrected geomagnetic latitudes: 65°-75°), has a local minimum at sub-auroral latitudes (55°-63°) and a low maximum at mid-latitudes (45°-50°). Thus, *Holappa et al.* (2014) states that the latitudinal effect of the second mode is caused by the difference between the average intensity and location between substorms related to HSSs and ICMEs.

Publication I studied the long-term evolution of the geomagnetic variations in the high-latitude regions using the International Monitor for Auroral Geomagnetic Effects (IMAGE) (*Viljanen and Häkkinen*, 1997) magnetometer array. Instead of using any existing geomagnetic index, the magnetic field variations were measured computing the daily standard deviation (STD) from the horizontal (X in Geographic coordinates) geomagnetic field component. By using the STD it was possible to divide the high-latitude region to even more narrower latitude bands than in the previous studies. It was shown in **Publication I** that even in the auroral region, there are variations in different latitudes to the response of different large-scale solar wind drivers (See Fig. 17). This means that when estimating the evolution of geomagnetic variations in a certain latitude band it can be more useful to estimate the disturbance level using single magnetometer station measurements instead of some known geomagnetic index.

6 Summary and Conclusions

This thesis consists of four published peer-reviewed research articles that are observationally studying the solar wind- magnetosphere system. The main motivation has been to understand how the solar wind conditions alter the coupling between the solar wind and magnetosphere. All these four publications aim to answer the main-level question: how does variable solar wind drive geomagnetic storms?

The publications use spacecraft and satellite data as well as ground-based magnetometer measurements. **Publications I, II, III and IV** are based on the solar wind data downloaded from NASA Goddard Space Flight Center's OMNIWeb (http://omniweb.gsfc.nasa.gov/). During the analysed periods the OMNI data consist mainly of Advanced Composition Explorer (ACE) and Wind satellite measurements. **Publication I** uses the one-hour resolution OMNI data while the other publications are using the one-minute time resolution data. **Publication II** also uses satellite data from the five THEMIS spacecraft that orbit the Earth at different distances. The study uses data from 2008 to 2011 when the satellite orbits covered the magnetotail from 4 to 30 R_E.

The magnetometer data in **Publication I** are from the IMAGE magnetometer network that is located in Fennoscandia and Svalbard. The time resolution of the geomagnetic field measurements is 10 seconds. Data set consist of 17 years of measurements from 15 magnetometer stations. The geomagnetic index data (AE, PCN and SYM-H) used in the **Publications II, III and IV** are also propagated through the OMNIWeb.

The next Section summaries the main conclusions of the thesis.

Results

Publication II combines the solar wind conditions with the magnetotail measurements to study the large-scale plasma transport. The sunward and tailward directed flows were studied separately. The statistical maps of the flow speeds and occurrences confirmed several features found in earlier studies as well as presented some

new features. **Publication II** also studied the effect of ultra low frequency B_Z power level to the occurrence of the plasma sheet flows, which, to the knowledge of the authors, has not been studied previously.

80 ICME events that consist of both sheath and magnetic cloud regions were analysed in the **Publication III** to study the solar wind-magnetosphere coupling efficiency. The events were selected so that either sheath or magnetic cloud (or both) drove a geomagnetic storm when Dst index was at least -50 nT. **Publication III** studied the effect of the solar wind parameters to the coupling efficiency as well as the differences of the results between the different definitions for the efficiency. The energy input was estimated using the interplanetary electric field dawn-dusk component (E_Y), as well as the Newell and Borovsky functions.

Publications II and III are both focused on the question, how solar wind-magnetosphere coupling efficiency, energy and plasma transport depend on solar wind parameters. While **Publication II** studied the effects of solar wind parameters to the plasma sheet at the magnetotail, **Publication III** highlighted the differences between the magnetospheric response in the polar cap convection, auroral electojets and ring current to the solar wind key-parameters.

It was shown in **Publication II** that the sunward flows vary greatly with the solar wind conditions while the tailward flow pattern is almost independent of the solar wind conditions. The sign of the IMF Z-component was noted to have the most visible effect on the occurrence rate and pattern of fast ($|V_{tail}| > 100$ km/s) sunward flows. The most unexpected observation was that the flow bursts exceeding > 100 km/s are more common during the slow solar wind conditions than during the fast solar wind. This needs to be studied more carefully in the future. However, it should be remembered that the results of **Publication II** were obtained using observations during mostly weakly driven magnetosphere during low solar activity period.

Publication III emphasized that the solar wind-magnetosphere coupling efficiency depends on the definition. It was observed that the E_Y and Newell functions give very similar results but the Borovsky function gives the most linear energy input during all solar wind conditions. However, when the PCN and AE index were used as the proxy for the energy output, they all saturated despite of the input estimate. Nevertheless, the Borovsky function showed less clear saturation for PCN than the E_Y and the Newell function.

Publications III and IV addressed the question what processes and parameters control the saturation of the polar cap potential.

Publication III showed that while the PCN and AE indices saturate when the solar wind driving increases, the SYM-H index does not. This is a sign that the ring current does not necessarily saturate either (*Lopez et al.*, 2009). The PCN and

AE saturation are both typically assumed to be related to the polar cap potential saturation. However, there is an interesting difference between the PCN and AE saturation: PCN is clearly Alfvén Mach number dependent while AE is not. PCN clearly saturates during low M_A conditions. Since PCN was assumed to be related to the CPCP, its low M_A saturation can be easily understood using the existing literature (e.g., *Lavraud and Borovsky*, 2008; *Lopez et al.*, 2010; *Wilder et al.*, 2011). **Publication III** also reported evidence of PCN saturation during high M_A (> 7.2) conditions. The saturation started to occur during more intense solar wind driving than the low M_A saturation. **Publication III** is the first study to suggest that CPCP saturation occurs during high M_A solar wind conditions.

Publication IV continued the study of the effect of solar wind parameters to the PCN index. Like in **Publication III**, PCN was assumed to be related to the CPCP. While the **Publication III** included only 80 ICME events, **Publication IV** used all OMNI data from the years 1986-2015 and thus the data set included also the non-storm periods. The study was focused particularly on the effect of the solar wind dynamic pressure to the PCN index. The main conclusions of **Publication IV** can be summarized as follows: 1) during high solar wind driving electric field, the PCN index increases with the increasing solar wind dynamic pressure, 2) velocity increases the coupling efficiency between the solar wind and the magnetosphere during all driving conditions and 3) removing the lowest Aflvén Mach number periods (< 5) from the data set does not remove the saturation effect from the PCN data. The meaning of the results of **Publication IV** in the context of the existing CPCP saturation models in the literature can be expressed simply by saying that such a model which could explain all the observed features of PCN does not exist.

The question, how large-scale solar wind driving affects the coupling efficiency and geomagnetic activity, motivated **Publications I and III**.

According to the results shown in **Publication III and IV** it is evident that solar wind - magnetosphere coupling efficiency, measured using the high-latitude indices, is higher during sheath region than magnetic cloud interactions. This follows from the results that the pressure is typically higher in sheath regions than magnetic clouds and increasing dynamic pressure increases polar cap potential. The CPCP saturation tends to also occur during low M_A solar wind that is typical for the magnetic clouds.

Publication I studied the long-term geomagnetic variations in the high-latitude region and compared the results with the abundance of different solar wind drivers. The previous studies, like *Finch et al.* (2008), have considered the auroral area (roughly the geomagnetic latitudes from 60° to 82°) as one region when studying the high-latitude response to the solar wind. This, however, neglects the possible latitudinal dependence of the drivers inside the auroral oval. It is shown in **Publi-**

cation I that there are, indeed, latitudinal differences in the magnetic disturbances inside the oval: the HSS activity affects most significantly to the northernmost part of the oval (magnetic latitudes $> 73.06°$) during the solar minimum and the region is the least responsive to the CME activity during the solar maximum. **Publication I** also demonstrates that the daily standard deviation is a useful measure to asses the geomagnetic disturbance level at a single magnetometer station. The measure is easy to compute and it does not require any baseline magnetic field subtraction.

As a by-product of the solar wind-magnetosphere coupling efficiency study in **Publication III** a new time delay analysis method was developed. When the solar wind - magnetosphere coupling is studied using data with a higher time resolution than one hour, the time lag between the solar wind and ground based measurements must be taken into account. There are several studies in the literature investigating the time lag between the geomagnetic indices and the solar wind drivers (e.g., *Bargatze et al.*, 1985; *Ridley et al.*, 1998; *Eriksson et al.*, 2000; *Stauning and Troshichev*, 2008). The magnetospheric system is also suggested to be insensitive to the smallest-scale fluctuations of the solar wind parameters and the magnetosphere is said to act as a low-pass filter (*Clauer et al.*, 1981; *Takalo et al.*, 2000; *Ilie et al.*, 2010). In contrast to previous methods that only searched for time delay between the solar wind and its magnetospheric response, the new method also investigates the optimal time window length, which is used to smooth the solar wind input parameters. Thus, the method takes into account both the time lag between cause and effect and the magnetospheric feature to act like a low-pass filter.

2 Future prospects

While writing the publications for the thesis, several new research questions and future interests arose. The cause of the CPCP saturation was unsolved before this PhD work was started and it still remains so. However, the thesis offered significant new information that can be used to distinguish between the existing saturation models and to exclude certain models. For example, based on the results presented in this PhD thesis, the saturation models that rely on the high dynamic pressure as a cause of the CPCP saturation can be rejected. **Publication III** revealed an unexpected feature of the solar wind-magnetosphere coupling during the ICME events: the saturation can also occur during times when the M_A is relatively high. This feature are poorly understood by the existing saturation models, which means that more theoretical work is needed to understand the saturation process.

The results shown in **Publication IV** can also be used to plan future MHD

simulation runs to examine the CPCP saturation problem and to verify the observed features of the CPCP. The MHD simulations, on the other hand, can offer important insight of the magnetospheric processes and the magnetosheath dynamics during the saturated magnetosphere. As observed in **Publication IV**, when the reconnection electric field was kept fixed the combination of higher velocity and smaller magnetic field lead to higher geomagnetic response in the polar region compared to the combination of the higher magnetic field and smaller velocity. This was true during all electric field strengths. The MHD simulations would be ideal to better understand and test the result.

So far, the CPCP saturation has been only studied using MHD simulations, which excludes all kinetic effects. In the future, it will be interesting to see if the hybrid simulations, like the Vlasiator (*Von Alfthan et al.*, 2014), are able to shed new light on the problem. Since the CPCP is directly related to the dayside reconnection, a more detailed understanding of the reconnection processes, which is achieved both by the hybrid simulations and NASA's Magnetospheric Multiscale (MMS, *Burch et al.* (2016)) mission, will benefit the understanding of the CPCP saturation as well. The saturation of the CPCP is also an important aspect for the generation of the extreme geomagnetic storms. Hence, a more detailed understanding of the processes in the magnetosphere during the saturation would improve the understanding of the most likely drivers of extreme storms and forecasting of these largest geospace disturbances.

The results shown in the thesis imply that the ICME sheath regions and interacting ICMEs that are typically associated with large dynamic pressure and strong magnetic fields are needed for driving the strongest geospace disturbances rather than the smooth flux rope part of the ICME, which may lead to the saturation of CPCP more easily and has generally the solar wind conditions associated with the lower coupling efficiency.

Bibliography

Abramenko, V., Yurchyshyn, V., Linker, J., Mikić, Z., Luhmann, J., and Lee, C. O. (2010), Low-latitude coronal holes at the minimum of the 23rd solar cycle, *The Astrophysical Journal*, 712(2), 813

Akasofu, S. I. (1981), Energy coupling between the solar wind and the magnetosphere, Space Science Reviews, 28(2), 121-190

Alfvén, H. (1942). Existence of electromagnetic-hydrodynamic waves. Nature, 150(3805), 405-406

American Association for the Advancement of Science, (1962). The Mission of Mariner II: Preliminary Observations Profile of Events, *Science*, 138(3545), 1095-1095

Angelopoulos, V., W. Baumjohann, C. F. Kennel, F. V. Coroniti, M. G. Kivelson, R. Pellat, R. J. Walker, H. Lühr, and G. Paschmann (1992), Bursty bulk flows in the inner central plasma sheet, *Journal of Geophysical Research*, 97(A4), 4027–4039, doi:10.1029/91JA02701

Angelopoulos, V., Kennel, C. F., Coroniti, F. V., Pellat, R., Spence, H. E., Kivelson, M. G., ... and Russell, C. T. (1993). Characteristics of ion flow in the quiet state of the inner plasma sheet, *Geophysical Research Letters*, 20(16), 1711-1714

Angelopoulos, V., C. F. Kennel, F. V. Coroniti, R. Pellat, M. G. Kivelson, R. J. Walker, C. T. Russell, W. Baumjohann, W. C. Feldman, and J. T. Gosling (1994), Statistical characteristics of bursty bulk flow events, *Journal of Geophysical Research*, 99(A11), 21257–21280, doi:10.1029/94JA01263

Angelopoulos, V. (2009), The THEMIS mission, *Springer New York*, pp. 5-34

Artusi, R., Verderio, P., and Marubini, E. (2002), Bravais-Pearson and Spearman correlation coefficients: meaning, test of hypothesis and confidence interval, *The International Journal of Biological Marker*, 17(2), 148-151

Axford, W. I., and Hines, C. O. (1961), A unifying theory of high-latitude geophysical phenomena and geomagnetic storms, *Canadian Journal of Physics*, 39(10), 1433-1464

Bame, S. J., Asbridge, J. R., Feldman, W. C., and Gosling, J. T. (1976), Solar cycle evolution of high-speed solar wind streams, *The Astrophysical Journal*, 207, 977-980

Bame, S. J., Goldstein, B. E., Gosling, J. T., Harvey, J. W., McComas, D. J., Neugebauer, M., and Phillips, J. L. (1993), Ulysses observations of a recurrent high speed solar wind stream and the heliomagnetic streamer belt, *Geophysical research letters*, 20(21), 2323–2326.

Bargatze, L. F., D. N. Baker, R. L. McPherron, and E. W. Hones Jr. (1985), Magnetospheric impulse response for many levels of geomagnetic activity, *Journal of Geophysical Research*, 90(A7), 6387–6394, doi:10.1029/JA090iA07p06387

Baumjohann, W., G. Paschmann, and H. Lühr (1990), Characteristics of high-speed ion flows in the plasma sheet, *Journal of Geophysical Research*, 95(A4), 3801–3809, doi:10.1029/JA095iA04p03801

Baumjohann, W., Kamide, Y., and Nakamura, R. (1996), Substorms, storms, and the near-Earth tail, *Journal of geomagnetism and geoelectricity*, 48(2), 177-185

Bhattarai, S. K., R. E. Lopez, R. Bruntz, J. G. Lyon, and M. Wiltberger (2012), Simulation of the polar cap potential during periods with northward interplanetary magnetic field, *Journal of Geophysical Research*, 117, A04219, doi:10.1029/2011JA017143

Biermann, L. (1957). Solar corpuscular radiation and the interplanetary gas. The Observatory, 77, 109-110

Borovsky, J. E., M. F. Thomsen, and D. J. McComas (1997), The superdense plasma sheet: Plasmaspheric origin, solar wind origin, or ionospheric origin?, *Journal of Geophysical Research*, 102(A10), 22089–22097, doi:10.1029/96JA02469

Borovsky, J. E., and Denton, M. H. (2006), Differences between CMEdriven storms and CIRdriven storms, *Journal of Geophysical Research: Space Physics*, 111(A7)

Borovsky, J. E. (2008), The rudiments of a theory of solar wind/magnetosphere coupling derived from first principles, *Journal of Geophysical Research: Space Physics*, 113(A8)

Borovsky, J. E., Lavraud, B., and Kuznetsova, M. M. (2009), Polar cap potential saturation, dayside reconnection, and changes to the magnetosphere, *Journal of Geophysical Research: Space Physics*, 114(A3)

Broussard, R. M., Sheeley, N. R., Tousey, R., and Underwood, J. H. (1978), A survey of coronal holes and their solar wind associations throughout sunspot cycle 20, *Solar Physics*, 56(1), 161-183.

Burch, J. L., Moore, T. E., Torbert, R. B., and Giles, B. L. (2016), Magnetospheric multiscale overview and science objectives, *Space Science Reviews*, 199(1-4), 5-21

Burlaga, L. F. (1988), Magnetic clouds and forcefree fields with constant alpha, *Journal of Geophysical Research: Space Physics (1978–2012)*, 93,A7, 7217–7224

Cassak, P. A., and Shay, M. A. (2007), Scaling of asymmetric magnetic reconnection: General theory and collisional simulations, *Physics of Plasmas*, 14(10), 102114

Chané, E., Saur, J., Neubauer, F. M., Raeder, J., and Poedts, S. (2012), Observational evidence of Alfvén wings at the Earth, *Journal of Geophysical Research: Space Physics*, 117(A9)

Clauer, C. R., McPherron, R. L., Searls, C., and Kivelson, M. G. (1981), Solar wind control of auroral zone geomagnetic activity, *Geophysical Research Letters*, 8(8), 915-918

Crooker, N. U. (1992), Reverse convection, *Journal of Geophysical Research: Space Physics*, 97(A12), 19363-19372

Davis, T. N., and M. Sugiura (1966), Auroral electrojet activity index AE and its universal time variations, *Journal of Geophysical Research*, 71(3), 785–801, doi:10.1029/JZ071i003p00785

Dimmock, A. P., K. Nykyri, H. Karimabadi, A. Osmane, and T. I. Pulkkinen (2015), A statistical study into the spatial distribution and dawn-dusk asymmetry of dayside magnetosheath ion temperatures as a function of upstream solar wind conditions, *Journal of Geophysical Research: Space Physics*, 120, 2767–2782, doi: 10.1002/2014JA020734

Dungey, J. W. (1961), Interplanetary magnetic field and the auroral zones, *Physical Review Letters*, 6(2), 47

Echer, E., Gonzalez, W. D., Gonzalez, A. L. C. D., Prestes, A., Vieira, L. E. A., Dal Lago, A., ... and Schuch, N. J. (2004), Long-term correlation between solar and geomagnetic activity, *Journal of Atmospheric and Solar-Terrestrial Physics*, 66(12), 1019-1025

Eriksson, S., R. E. Ergun, C. W. Carlson, and W. Peria (2000), The cross-polar potential drop and its correlation to the solar wind, *Journal of Geophysical Research*, 105(A8), 18,639–18,653, doi:10.1029/2000JA900033

Fairfield, D. H., R. P. Lepping, E. W. Hones Jr., S. J. Bame, and J. R. Asbridge (1981), Simultaneous measurements of magnetotail dynamics by IMP spacecraft, *Journal of Geophysical Research*, 86(A3), 1396–1414, doi:10.1029/JA086iA03p01396

Finch, I. D., M. L. Lockwood, and A. P. Rouillard (2008), Effects of solar wind magnetosphere coupling recorded at different geomagnetic latitudes: Separation of directly-driven and storage/release systems, *Geophysical Research Letters*, 35, L21105, doi:10.1029/2008GL035399

Foullon, C., C. J. Farrugia, A. N. Fazakerley, C. J. Owen, F. T. Gratton, and R. B. Torbert (2008), Evolution of Kelvin-Helmholtz activity on the dusk flank magnetopause, *Journal Geophysical Researc*, 113, A11203, doi:10.1029/2008JA013175

Fu, H. S., Y. V. Khotyaintsev, A. Vaivads, M. André, and S. Y. Huang (2012), Occurrence rate of earthward-propagating dipolarization fronts, *Geophysical Research Letters*, 39, L10101, doi:10.1029/2012GL051784

Georgieva, K., Kirov, B., and Gavruseva, E. (2006), Geoeffectiveness of different solar drivers, and long-term variations of the correlation between sunspot and geomagnetic activity, *Physics and Chemistry of the Earth*, Parts A/B/C, 31(1), 81-87

Gonzalez, W. D., Tsurutani, B. T., and Clúa de Gonzalez, A. L. (1999), Interplanetary origin of geomagnetic storms, *Space Science Reviews*, 88(3), 529-562

Guo, J., Feng, X., Emery, B. A., Zhang, J., Xiang, C., Shen, F., and Song, W. (2011), Energy transfer during intense geomagnetic storms driven by interplanetary coronal mass ejections and their sheath regions, *Journal of Geophysical Research: Space Physics*, 116(A5)

Hill, T. W., Dessler, A. J., and Wolf, R. A. (1976), Mercury and Mars: The role of ionospheric conductivity in the acceleration of magnetospheric particles, *Geophysical Research Letters*, 3(8), 429–432

Holappa, L., Mursula, K., Asikainen, T., and Richardson, I. G. (2014), Annual fractions of highspeed streams from principal component analysis of local geomagnetic activity, *Journal of Geophysical Research: Space Physics*, 119(6), 4544–4555

Holappa, L., Mursula, K., and Asikainen, T. (2014), A new method to estimate annual solar wind parameters and contributions of different solar wind structures to geomagnetic activity, *Journal of Geophysical Research: Space Physics*, 119(12), 9407–9418

Huttunen, K. E. J., Koskinen, H. E., and Schwenn, R. (2002), Variability of magnetospheric storms driven by different solar wind perturbations, *Journal of Geophysical Research: Space Physics*, 107(A7)

Huttunen, K. E. J and Koskinen, H. E. (2004), Importance of post-shock streams and sheath region as drivers of intense magnetospheric storms and high-latitude activity, *Annales Geophysicae*, 22 (5), 1729-1738

Huttunen, K. E. J., H. E. J. Koskinen, A. Karinen, and K. Mursula (2006), Asymmetric development of magnetospheric storms during magnetic clouds and sheath regions, *Geophysical Research Letters*, 33, L06107, doi:10.1029/2005GL024894

Ilie, R., Liemohn, M. W., and Ridley, A. (2010), The effect of smoothed solar wind inputs on global modeling results, *Journal of Geophysical Research: Space Physics*, 115(A1)

Iyemori, T. (1990), Storm-time magnetospheric currents inferred from mid-latitude geomagnetic field variations, *Journal of geomagnetism and geoelectricity*, 42(11), 1249-1265

Juusola, L., N. Østgaard, and E. Tanskanen (2011), Statistics of plasma sheet convection, *Journal of Geophysical Research*, 116, A08201, doi:10.1029/2011JA016479

Kamide, Y., et al. (1998), Current understanding of magnetic storms: Storm-substorm relationships, *Journal of Geophysical Research*, 103(A8), 17705–17728, doi:10.1029/98JA01426

Kamide, Y., and S. Kokubun (1996), Two-component auroral electrojet: Importance for substorm studies, *Journal of Geophysical Research.*, 101(A6), 13027–13046, doi:10.1029/96JA00142

Kan, J. R., and Lee, L. C. (1979), Energy coupling function and solar windmagnetosphere dynamo, *Geophysical Research Letters*, 6(7), 577-580

Kilpua, E. K. J., Hietala, H., Koskinen, H. E. J., Fontaine, D., and Turc, L. (2013), Magnetic field and dynamic pressure ULF fluctuations in coronal-mass-ejection-driven sheath regions, *Annales Geophysicae*, 31, 1559-1567, doi:10.5194/angeo-31-1559-2013

Kivelson, M. G., and Ridley, A. J. (2008), Saturation of the polar cap potential: Inference from Alfvén wing arguments, *Journal of Geophysical Research: Space Physics*, 113(A5)

Koskinen, H. E. J. (2011),*Physics of space storms: From the solar surface the Earth*, Berlin; London; Chichester, UK: Springer; Published in association with Praxis Pub, ISBN: 978-3-642-00310-3

Lavraud, B., and Borovsky, J. E. (2008), Altered solar windmagnetosphere interaction at low Mach numbers: Coronal mass ejections, *Journal of Geophysical Research: Space Physics*, 113(A9)

Lopez, R. E., Lyon, J. G., Mitchell, E., Bruntz, R., Merkin, V. G., Brogl, S., ... and Wiltberger, M. (2009), Why doesn't the ring current injection rate saturate?, *Journal of Geophysical Research: Space Physics*, 114(A2)

Lopez, R. E., Bruntz, R., Mitchell, E. J., Wiltberger, M., Lyon, J. G., and Merkin, V. G. (2010), Role of magnetosheath force balance in regulating the dayside reconnection potential, *Journal of Geophysical Research: Space Physics*, 115(A12)

Luhmann, J. G., Walker, R. J., Russell, C. T., Crooker, N. U., Spreiter, J. R., and Stahara, S. S. (1984), Patterns of potential magnetic field merging sites on the dayside magnetopause, *Journal of Geophysical Research: Space Physics*, 89(A3), 1739-1742.

Lundin, R., and Evans, D. S. (1985), Boundary layer plasmas as a source for high-latitude, early afternoon, auroral arcs, *Planetary and space science*, 33(12), 1389-1406

Mavromichalaki, H., and Vassilaki, A. (1998), Fast plasma streams recorded near the Earth during 1985–1996, *Solar Physics*, 183(1), 181-200

Mayaud, P. N. (1980), Derivation, meaning, and use of geomagnetic indices, *Washington DC American Geophysical Union Geophysical Monograph Series*, 22

Nagai, T., Fujimoto, M., Saito, Y., Machida, S., Terasawa, T., Nakamura, R., ... and Kokubun, S. (1998), Structure and dynamics of magnetic reconnection for substorm onsets with Geotail observations, *Journal of Geophysical Research: Space Physics*, 103(A3), 4419-4440.

Nakamura, R., Baumjohann, W., Klecker, B., Bogdanova, Y., Balogh, A., Reme, H., ... and Kistler, L. (2002), Motion of the dipolarization front during a flow burst event observed by Cluster, *Geophysical research letters*, 29(20)

Neubauer, F. M. (1980), Nonlinear standing Alfvén wave current system at Io: Theory, *Journal of Geophysical Research: Space Physics*, 85(A3), 1171-1178

Newell, P. T., Sotirelis, T., Liou, K., Meng, C. I., and Rich, F. J. (2007), A nearly universal solar windmagnetosphere coupling function inferred from 10 magnetospheric state variables, *Journal of Geophysical Research: Space Physics*, 112(A1)

Nykyri, K. and Otto, A. (2001), Plasma transport at the magnetospheric boundary due to reconnection in Kelvin-Helmholtz vortices, *Geophysical Research Letters*, 28: 3565–3568. doi:10.1029/2001GL013239

Parker, E. N. (1957), Sweet's mechanism for merging magnetic fields in conducting fluids, *Journal of Geophysical Research*, 62(4), 509-520

Parker, E. N. (1958), Dynamics of the interplanetary gas and magnetic fields, *The Astrophysical Journal*, 128, 664

Partamies, N., Pulkkinen, T. I., McPherron, R. L., McWilliams, K., Bryant, C. R., Tanskanen, E., ... and Thomsen, M. F. (2009), Different magnetospheric modes: solar wind driving and coupling efficiency, *Annales Geophysicae*, 27, 11, 4281–4291

Partamies, N., Juusola, L., Tanskanen, E., and Kauristie, K. (2013), Statistical properties of substorms during different storm and solar cycle phases, *Annales Geophysicae*, 31, 2, 349

Perreault, P., and Akasofu, S. I. (1978), A study of geomagnetic storms. Geophysical Journal International, 54(3), 547-573

Phillips, J. L., Balogh, A., Bame, S. J., Goldstein, B. E., Gosling, J. T., Hoeksema, J. T., ... and Wang, Y. M. (1994), Ulysses at 50 south: constant immersion in the highspeed solar wind, *Geophysical research letters*, 21(12), 1105–1108

Pontius, D. H., and Wolf, R. A. (1990), Transient flux tubes in the terrestrial magnetosphere, *Geophysical research letters*, 17(1), 49-52

Raeder, J., and Lu, G. (2005), Polar cap potential saturation during large geomagnetic storms, *Advances in Space Research*, 36(10), 1804-1808

Reiff, P. H., Spiro, R. W., and Hill, T. W. (1981), Dependence of polar cap potential drop on interplanetary parameters, *Journal of Geophysical Research: Space Physics (1978–2012)*, 86(A9), 7639–7648

Reiff, P. H., and Luhmann, J. G. (1986), Solar wind control of the polar-cap voltage, *In Solar wind magnetosphere coupling*, Vol. 126, pp. 453–476

Richardson, I. G., Cliver, E. W., and Cane, H. V. (2001), Sources of geomagnetic storms for solar minimum and maximum conditions during 1972–2000, *Geophysical Research Letters*, 28(13), 2569-2572

Richardson, I. G., Cane, H. V., and Cliver, E. W. (2002), Sources of geomagnetic activity during nearly three solar cycles (1972–2000), *Journal of Geophysical Research: Space Physics*, 107(A8)

Ridley, A. J., G. Lu, C. R. Clauer, and V. O. Papitashvili (1998), A statistical study of the ionospheric convection response to changing interplanetary magnetic field conditions using the assimilative mapping of ionospheric electrodynamics technique, *Journal of Geophysical Research*, 103(A3), 4023–4039, doi:10.1029/97JA03328

Ridley, A. J., and Kihn, E. A. (2004), Polar cap index comparisons with AMIE cross polar cap potential, electric field, and polar cap area, *Geophysical research letters*, 31(7)

Ridley, A. J. (2005). A new formulation for the ionospheric cross polar cap potential including saturation effects. In Annales Geophysicae (Vol. 23, No. 11, pp. 3533-3547)

Ridley, A. J. (2007), Alfvén wings at Earth's magnetosphere under strong interplanetary magnetic fields, *Annales Geophysicae* 25, 2, 533-542

Riley, P., Luhmann, J. G. (2012). Interplanetary signatures of unipolar streamers and the origin of the slow solar wind. Solar Physics, 277(2), 355-373

Rostoker, G. (1972), Geomagnetic indices, *Rev. Geophys.*, 10(4), 935–950, doi:10.1029/RG010i004p00935

Rostoker, G., Akasofu, S. I., Foster, J. C., Greenwald, R. A., Kamide, Y., Kawasaki, K., ... and Russell, C. T. (1980), Magnetospheric substorms—Definition and signatures, *Journal of Geophysical Research: Space Physics*, 85(A4), 1663-1668

Russell, C. T., Luhmann, J. G., and Lu, G. (2001), Nonlinear response of the polar ionosphere to large values of the interplanetary electric field, *Journal of Geophysical Research: Space Physics (1978–2012)*, 106(A9), 18495–18504

Shepherd, S. G. (2007), Polar cap potential saturation: Observations, theory, and modeling, *Journal of Atmospheric and Solar-Terrestrial Physics*, 69(3), 234–248

Shiokawa, K., Baumjohann, W., and Haerendel, G. (1997), Braking of highspeed flows in the nearEarth tail, *Geophysical research letters*, 24(10), 1179-1182

Siscoe, G. L., Erickson, G. M., Sonnerup, B. Ö., Maynard, N. C., Schoendorf, J. A., Siebert, K. D., ... and Wilson, G. R. (2002), Hill model of transpolar potential saturation: Comparisons with MHD simulations, *Journal of Geophysical Research: Space Physics*, 107(A6)

Siscoe, G. L., Crooker, N. U., and Siebert, K. D. (2002), Transpolar potential saturation: Roles of region 1 current system and solar wind ram pressure, *Journal of Geophysical Research: Space Physics*, 107(A10)

Slavin, J. A., Tsurutani, B. T., Smith, E. J., Jones, D. E. and Sibeck, D. G. (1983), Average configuration of the distant (<220 Re) magnetotail: Initial ISEE-3 magnetic field results, *Geophysical Research Letters*, 10: 973–976. doi:10.1029/GL010i010p00973

Slavin, J. A., Lepping, R. P., Gjerloev, J., Fairfield, D. H., Hesse, M., Owen, C. J., ... and Mukai, T. (2003), Geotail observations of magnetic flux ropes in the plasma sheet, *Journal of Geophysical Research: Space Physics*, 108(A1)

Sonnerup, B. U. (1970), Magnetic-field re-connexion in a highly conducting incompressible fluid, *Journal of Plasma Physics*, 4(01), 161-174

Sonnerup, B. U. (1974), Magnetopause reconnection rate, *Journal of Geophysical Research*, 79(10), 1546-1549

Stauning, P., and O. A. Troshichev (2008), Polar cap convection and PC index during sudden changes in solar wind dynamic pressure, *Journal of Geophysical Research*, 113, A08227, doi:10.1029/2007JA012783

Strangeway, R. J., R. C. Elphic, W. J. Peria, and C. W. Carlson (2000), FAST observations of electromagnetic stresses applied to the polar ionosphere, in Magnetospheric Current Systems, Geophys. Monogr. Ser., vol. 118, edited by S. Ohntani et al., pp. 21–29, AGU, Washington, D. C., doi:10.1029/GM118p0021

Sugiura, M., and Kamei, T. (1991), Equatorial Dst Index: 1957-1986. A. Berthelier, and M. Menvielle (Eds.). ISGI Publications Office.

Sundberg, K. Å. T., J. A. Cumnock, and L. G. Blomberg (2009), Reverse convection potential: A statistical study of the general properties of lobe reconnection and saturation effects during northward IMF, *Journal of Geophysical Research*, 114, A06205, doi:10.1029/2008JA013838

Sweet, P. A. (1958). 14. The neutral point theory of solar flares. *In Symposium-International Astronomical Union* (Vol. 6, pp. 123-134). Cambridge University Press

Takalo, J., Mursula, K., and Timonen, J. (2000), Role of the driver in the dynamics of a coupled-map model of the magnetotail - Does the magnetosphere act as a low-pass filter?, *Journal of geophysical research*, 105, 27

Tanskanen, E., T. I. Pulkkinen, H. E. J. Koskinen, and J. A. Slavin (2002), Substorm energy budget during low and high solar activity: 1997 and 1999 compared, *Journal of Geophysical Research*, 107(A6), doi:10.1029/2001JA900153

Tanskanen, E. I. (2009), A comprehensive highthroughput analysis of substorms observed by IMAGE magnetometer network: Years 1993–2003 examined, *Journal of Geophysical Research: Space Physics*, 114(A5)

Trattner, K. J., J. S. Mulcock, S. M. Petrinec, and S. A. Fuselier (2007), Probing the boundary between antiparallel and component reconnection during southward interplanetary magnetic field conditions, *Journal of Geophysical Research.*, 112, A08210, doi:10.1029/2007JA012270

Troshichev, O. A., Dmitrieva, N. P., and Kuznetsov, B. M. (1979), Polar cap magnetic activity as a signature of substorm development, *Planetary and Space Science*, 27(3), 217-221.

Troshichev, O. A., Andrezen, V. G., Vennerstrøm, S., and Friis-Christensen, E. (1988), Magnetic activity in the polar cap—A new index, *Planetary and space science*, 36(11), 1095-1102

Troshichev, O., Hayakawa, H., Matsuoka, A., Mukai, T., and Tsuruda, K. (1996), Cross polar cap diameter and voltage as a function of PC index and interplanetary quantities, *Journal of Geophysical Research: Space Physics*, 101(A6), 13429-13435

Turner, N. E., Cramer, W. D., Earles, S. K., and Emery, B. A. (2009), Geoefficiency and energy partitioning in CIR-driven and CME-driven storms, *Journal of Atmospheric and Solar-Terrestrial Physics*, 71(10), 1023-1031

Viljanen, A. and Häkkinen, L. (1997), IMAGE magnetometer network, *Satellite-ground based coordination sourcebook*, 1198, 111

Von Alfthan, S., Pokhotelov, D., Kempf, Y., Hoilijoki, S., Honkonen, I., Sandroos, A., and Palmroth, M. (2014), Vlasiator: First global hybrid-Vlasov simulations of Earth's foreshock and magnetosheath, *Journal of Atmospheric and Solar-Terrestrial Physics*, 120, 24-35

Wang, Y. M., and Sheeley Jr, N. R. (1990), Solar wind speed and coronal flux-tube expansion, *The Astrophysical Journal*, 355, 726-732

Wang, Y. M., Sheeley Jr, N. R., Walters, J. H., Brueckner, G. E., Howard, R. A., Michels, D. J., ... and Simnett, G. M. (1998), Origin of streamer material in the outer corona, *The Astrophysical Journal Letters*, 498(2), L165

Wang, C. P., Lyons, L. R., Weygand, J. M., Nagai, T., and McEntire, R. W. (2006), Equatorial distributions of the plasma sheet ions, their electric and magnetic drifts, and magnetic fields under different interplanetary magnetic field Bz conditions, *Journal of Geophysical Research: Space Physics*, 111(A4)

Wanliss, J. A., and Showalter, K. M. (2006), Highresolution global storm index: Dst versus SYMH, *Journal of Geophysical Research: Space Physics*, 111(A2)

Weimer, D. R., L. A. Reinleitner, J. R. Kan, L. Zhu, and S.-I. Akasofu (1990), Saturation of the auroral electrojet current and the polar cap potential, *J. Geophys. Res.*, 95(A11), 18981–18987, doi:10.1029/JA095iA11p18981

Wilder, F. D., C. R. Clauer, and J. B. H. Baker (2008), Reverse convection potential saturation during northward IMF, Geophysical Research Letters, 35, L12103, doi:10.1029/2008GL034040

Wilder, F. D., Clauer, C. R., Baker, J. B. H., Cousins, E. P., and Hairston, M. R. (2011), The nonlinear response of the polar cap potential under southward IMF: A statistical view, *Journal of Geophysical Research: Space Physics*, 116(A12)

Wilder, F. D., S. Eriksson, and M. Wiltberger (2015), The role of magnetic flux tube deformation and magnetosheath plasma beta in the saturation of the Region

1 field-aligned current system, *Journal of Geophysical Research, Space Physics*, 120, 2036–2051. doi: 10.1002/2014JA020533

Xystouris, G., Sigala, E., and Mavromichalaki, H. (2014), A complete catalogue of high-speed solar wind streams during solar cycle 23, *Solar Physics*, 289(3), 995-1012

Yermolaev, Y. I., Nikolaeva, N. S., Lodkina, I. G., and Yermolaev, M. Y. (2012), Geoeffectiveness and efficiency of CIR, sheath, and ICME in generation of magnetic storms, *Journal of Geophysical Research: Space Physics*, 117(A9)

Zhang, J., Liemohn, M. W., Kozyra, J. U., Thomsen, M. F., Elliott, H. A., and Weygand, J. M. (2006), A statistical comparison of solar wind sources of moderate and intense geomagnetic storms at solar minimum and maximum, *Journal of Geophysical Research: Space Physics*, 111(A1